3-27-2020 2:30 PM

Lateral Load Analysis of Multi-Storey Light-Frame Wood Buildings through Detailed and Simplified Numerical Approaches

Chu Peng, *The University of Western Ontario*

Supervisor: El Damatty, Ashraf A., *The University of Western Ontario*

A thesis submitted in partial fulfillment of the requirements for the Master of Engineering Science degree in Civil and Environmental Engineering

Abstract

Increasing global demand for a sustainable society is driving the development of multi-storey light-frame wood structures (LFWSs). A high-resolution finite element modelling (FEM) procedure for three-dimensional multi-storey LFWS buildings is developed. This tremendous effort is carried out to have a benchmark model that can be used for the validation of simpler models and for the assessment of the structural performance considering system effects. High-resolution FEM of all components of a building is not practical. A simplified FEM procedure is developed based on equal work principle. Verification of the accuracy of the high-resolution model is undertaken by comparing the natural frequencies predicted by the high-resolution model and a full-scale field measurement. Also, pushover curves obtained from both the simplified and the high-resolution building models are compared. It is demonstrated that the simplified FEM can predict accurately the behaviour of multi-storey single walls as well as an entire building with good accuracy compared to the high-resolution FEM.

Keywords

Light-frame wood structure, three-dimensional high-resolution modelling, three-dimensional simplified modelling, pushover analysis, structural performance, system effect

Summary for Lay Audience

About ninety percent of North America's residential buildings consist of light-frame wood structures (LFWSs). Wood is a renewable, recyclable, and biodegradable material. Promoting the development of LFWS buildings aligns with the global demand for a sustainable society. Current limitation on the advancement of LFWSs is the deficiency of the design method, which is a hand-calculation-based design at the individual member level rather than an advanced computer-aided design at the entire building level. Hand-calculation-based design makes the LFWSs either unsafe or too conservative (costly), thus unideal. However, due to the complex structural details of LFWSs, computer-aided design of LFWS buildings with all structural components modelled are not practical. This research aims at finding an effective simplified computer-aided design approach for LFWSs so that practical engineers in industry can easily perform the design process without modelling all complex structural details. To fulfill this objective, a high-resolution model with the consideration of all structural components is first completed with the help of a computer. This tremendous effort is carried out to have a benchmark model that can be used for the validation of simpler models. The accuracy of this high-resolution model is verified through a full-scale field test. The structural behaviour of this high-resolution model is also investigated to better understand the performance of LFWSs at three-dimensional level. Subsequently, a simplified model is proposed with the help of a computer. The simplified model is validated capable of yielding similar lateral displacement prediction compared to the high-resolution model if a lateral force is applied to the model that simulates a LFWS building.

Co-Authorship Statement

This thesis has been prepared in accordance with the regulations for an Integrated Article format thesis stipulated by the School of Graduate and Postdoctoral Studies at Western University. Statements of the co-authorship of individual chapters are as follows:

Chapter 2: Simplified Numerical Approach for the Lateral Load Analysis of Light-Frame Wood Shear Wall Structures

The initial simplified numerical model was proposed by Dr. A. A. El Damatty. Modifications to the simplified numerical model and validation of the modified simplified numerical model against the high-resolution numerical model were completed by C. Peng and Dr. A. Musa under the continuous assistance of the supervisor Dr. A. A. El Damatty with the co-operation with Dr. A. Hamada.

Drafts of the Chapter 2 were written by C. Peng, and modifications were done under the supervision of Dr. A. A. El Damatty. A paper co-authored by C. Peng, A. A. El Damatty, A. Musa, and A. Hamada has been submitted to the *Engineering Structures*.

Chapter 3: High-resolution and Simplified Numerical Modelling of a Four-Storey Light-Frame Wood Building

The field test of a building was performed by Dr. A. Sadhu and his students. The high-resolution three-dimensional numerical model of the building, the high-resolution three-dimensional numerical model's structural performance analysis, and the development and validation of the simplified three-dimensional numerical model were conducted by C. Peng under the close supervision of Dr. A. A. El Damatty with the co-operation with Dr. A. Hamada regarding industrial practices.

Acknowledgments

The completion of this research was made possible with the invaluable guidance and financial assistance from my supervisor Prof. Ashraf El Damatty. I felt grateful for your continuous motivation, encouragement, and guidance towards my degree. I would also like to thank Western University, SBM Inc., and Mitacs for funding this research.

Thank you to Dr. Ahmed Hamada for providing me with many invaluable industrial practices and editing my conference papers. I would also like to express my gratitude to Dr. Ahmed Musa and Mohammad Niazi for your generous assistance to this research. I am also grateful for Dr. Ayan Sadhu for the wonderful collaboration in the field test.

I would also like to extend a special thank you to Haoyi Zhang, Zinan (Wilson) Wu, Miaolin Zhong, Pengpeng He, and Shucheng (Steve) Yang for your time and inspiring discussions with me related to this research. Thank you to my other friends Biyi Li, Gaoqi Rao, Jiahao Wang, Lin Sun, Wenjuan Mu, Yi Liu, and Zhenchao Le for being trustworthy, having lunch with you is usually my highlight and most expected moment in a day throughout this journey. I would also like to thank you to my other teammates Sébastien Maheux, Ibrahim Ibrahim, Mohamed AbuGazia, Moustafa El Assaly, Wesam AbdElhamid Mohamed, Adnan Enajar, Ahmed Shehata, Mostafa Ahmed, and Nima Ezami for the friendship.

Finally, I would like to express my deepest gratitude to my parents and my elder sister. Your continuous support and encouragement throughout my educational life has allowed me to pursue this prestigious degree.

Table of Contents

Abstract ii

Summary for Lay Audience iii

Co-Authorship Statement iv

Acknowledgments v

Table of Contents vi

List of Tables ix

List of Figures x

List of Symbols and Abbreviations xiii

Chapter 1 1

1 Introduction 1

1.1 Motivation 1

1.2 Background 2

1.2.1 High-resolution FEM of LFWS single shear walls 3

1.2.2 High-resolution FEM of three-dimensional LFWS buildings 4

1.2.3 Simplified FEM of LFWS single shear walls 4

1.2.4 Simplified FEM of three-dimensional LFWS buildings 6

1.3 Objective of the study 8

1.4 Thesis structure 8

1.4.1 Simplified numerical approach for the lateral load analysis of light-frame wood shear wall structures 9

1.4.2 High-resolution and simplified numerical modelling of a four-storey light-frame wood building 9

1.5 References 10

Chapter 2 14

2 Simplified Numerical Approach for the Lateral Load Analysis of Light-Frame Wood Shear Wall Structures 14

2.1 Introduction 14

2.2 Overview of the adopted FEM modelling procedure 19

2.3 Simplified modelling procedure 21

2.3.1 Modelling procedure 22

2.3.2 Effect of the gravity load F_V 26

2.3.3 Effect of the tie rods 27

2.4 Simplified modelling for single-storey single walls 27

2.4.1 Details of the six walls studied 27

2.4.2 Displacement component 31

2.4.3 Spring characteristics 33

2.4.4 Validation of the simplified model results 36

2.4.5 Single-storey single-wall simplified model database 38

2.5 Simplified modelling for a multi-storey single wall 38

2.5.1 Floor connection 38

2.5.2 Modelling procedure 39

2.5.3 Analysis results 40

2.6 Summary and conclusions 45

2.7 References 47

Chapter 3 50

3 High-Resolution and Simplified Numerical Modelling of a Four-Storey Light-Frame Wood Building 50

3.1 Introduction 50

3.2 Description of the structural system of an actual LFWS building 53

3.3 Description of the high-resolution FEM 57

3.3.1 Material properties 58

3.3.2 Nail modelling 59
3.3.3 Tie rod modelling 59
3.3.4 Shell element modelling 59
3.3.5 Shear wall connectivity at adjacent storeys 60
3.4 Validation of the high-resolution FEM through field measurement 60
3.5 Simplified three-dimensional four-storey model 63
3.6 Structural performance of the high-resolution model under design loads 64
3.7 Summary and conclusions 68
3.8 References 69
Chapter 4 73
4 Conclusions and Recommendations for Future Work 73
4.1 Conclusions 73
4.2 Recommendations for future work 76
Curriculum Vitae 78

List of Tables

Table 2-1: Characteristics of the six shear walls studied 29

Table 2-2: Material properties of the frame and the OSB panel (Mi, 2004; Winkel, 2006)... 30

Table 3-1: Schedules of end posts and nail spacing 55

Table 3-2: Schedule of the stud 55

Table 3-3: Details of all of the shear walls. 56

Table 3-4: Gravity load details (Unit: kPa)..... 57

Table 3-5: Frequencies comparison 63

Table 3-6: Maximum demand-to-capacity ratios of the sheathing panels of W9..... 67

Table 3-7: Maximum demand-to-capacity ratios of the frame members of W9 68

List of Figures

Figure 1-1: LFWS Shear Wall and Roof Structural Details (Satheeskumar et al., 2017) 2

Figure 2-1: Common components of a LFWS..... 16

Figure 2-2: (a) Shear wall high-resolution FEM model details and (b) its pushover result compared with the experimental findings (Niazi et al., 2018)..... 20

Figure 2-3: Simplified "two-link" model: (a) simplified model flexural springs; (b) simplified model shear springs..... 21

Figure 2-4: Flowchart of the simplified FEM procedure..... 23

Figure 2-5: Component of the pushover analysis result 26

Figure 2-6: Consideration of the gravitational load in ETABS (CSI, 2016) 27

Figure 2-7: Structural details of the W_S shear wall (dimensions: mm)..... 28

Figure 2-8: FF nail properties: (a) axial tensile behaviour; (b) shear behaviour (Winkel, 2006) 30

Figure 2-9: Shear properties of SF nails (Winkel, 2006)..... 30

Figure 2-10: Displacement components: (a) W_S; (b) W_{ST}; (c) W_{SV}; (d) W_L; (e) W_{LT}; (f) W_{LV} . 32

Figure 2-11: Spring characteristics: axial (a) and shear (b) properties of W_S; axial (c) and shear (d) properties of W_{ST}; axial (e) and shear (f) properties of W_{SV}; axial (g) and shear (h) properties of W_L; axial (i) and shear (j) properties of W_{LT}; axial (k) and shear (l) properties of W_{LV}..... 36

Figure 2-12: Validation of the simplified model results for (a) W_S ; (b) W_{ST}; (c) W_{SV}; (d) W_L; (e) W_{LT}; (f) W_{LV} 37

Figure 2-13: Connection between two adjacent storeys in the high-resolution FEM..... 39

Figure 2-14: Multi-storey simplified model 40

Figure 2-15: Comparison of high-resolution and simplified analysis results for the W_S type of four-storey shear wall: (a) fourth storey; (b) third storey; (c) second storey; (d) first storey. 41

Figure 2-16: Comparison of high-resolution and simplified analysis results for the W_L type of four-storey shear wall: (a) fourth storey; (b) third storey; (c) second storey; (d) first storey. 42

Figure 2-17: Comparison of high-resolution and simplified analysis results for W_{ST} type four-storey shear wall: (a) fourth storey; (b) third storey; (c) second storey; (d) first storey..... 43

Figure 2-18: Comparison of high-resolution and simplified analysis results for W_{LT} type four-storey shear wall: (a) fourth storey; (b) third storey; (c) second storey; (d) first storey..... 44

Figure 3-1: Composite wood-on-concrete building..... 54

Figure 3-2: Floor plans..... 56

Figure 3-3: High-resolution building model..... 58

Figure 3-4: Sensor instrumentation plan..... 61

Figure 3-5: On-site sensor instrumentation..... 61

Figure 3-6: Time history of physical response of the top floor of the building..... 62

Figure 3-7: Fourier Spectra of modal responses obtained from the field measurement for the first two modes..... 62

Figure 3-8: Simplified four-storey model..... 64

Figure 3-9: Simplified model rigid diaphragm 64

Figure 3-10: Comparison of pushover analyses results for both the high-resolution and simplified model 64

Figure 3-11: Consideration of load combination..... 65

Figure 3-12: Nail deformation under design loads: vertical-shear direction (a) and horizontal-shear direction (b) of SF; axial-tension direction (c), in-plane shear direction (d), and out-of-plane shear direction (e) of FF 66

List of Symbols and Abbreviations

3D	Three-dimensional
b	Shear wall width
d	Lateral total displacement
d_c	Stud vertical compressive displacement
d_f	Lateral flexural displacement component
DOFs	Degrees-of-freedoms
d_s	Lateral shear displacement component
d_t	Stud vertical tensile displacement
d_v	Relative vertical displacement of the side-studs
FEM	Finite element modelling
FF	Framing-to-framing
F_V	Gravity load
GWB	Gypsum wall board
h	Shear wall height
k_c	Equivalent compressive stiffness
k_s	Equivalent shear stiffness
k_t	Equivalent tensile stiffness
LFWSs	Light-frame wood structures
OSB	Oriented strand board

P	Base shear
P_c	Applied downward load
SF	Sheathing-to-framing
SPF	Spruce-pine-fir
ΔC	Incremental link compressive force
Δd_{fi}	Incremental lateral flexural displacement
ΔP_i	Incremental base shear
ΔT	Incremental link tensile force
Δu_c	Incremental link compressive displacement
Δu_t	Incremental link tensile displacement
Δd_{si}	Incremental lateral shear displacement

Chapter 1

1 Introduction

1.1 Motivation

About ninety percent of North America's residential buildings consist of light-frame wood structures (LFWSs). Wood is a renewable, recyclable, and biodegradable material. Compared to manufactured materials such as concrete and steel, two commonly used materials nowadays, wood has less environmental cost in its extraction, manufacture and transport. Wood can absorb CO_2 in the process of its growing, which can reduce the greenhouse effect. Moreover, wood structure construction takes less time than the construction of concrete and steel structures, which further features wood as a green material.

Being an environment-friendly material, wood is becoming more popular in midrise building construction around the world. The National Building Code of Canada (NBCC, 2015) allows up to six storeys of LFWSs, an increase from the previous code provision that limited LFWSs to four storeys. However, the complex structural components (Figure 1-1) especially the fasteners make the high-resolution finite element modelling (FEM) and analysis of LFWS buildings time-consuming, which makes the computer-aided design of LFWS buildings not practical for industrial application. Current design method of LFWS buildings adopted in industry is based on hand-calculation of individual structural subassembly, which makes the design either unsafe or too conservative. Moreover, the design of a three-dimensional (3D) LFWS building on the individual subassembly design basis without the consideration of system effect cannot accurately assess the behaviour of LFWS buildings with complex structural system which comprise numerous subassemblies connected together to resist the applied loads.

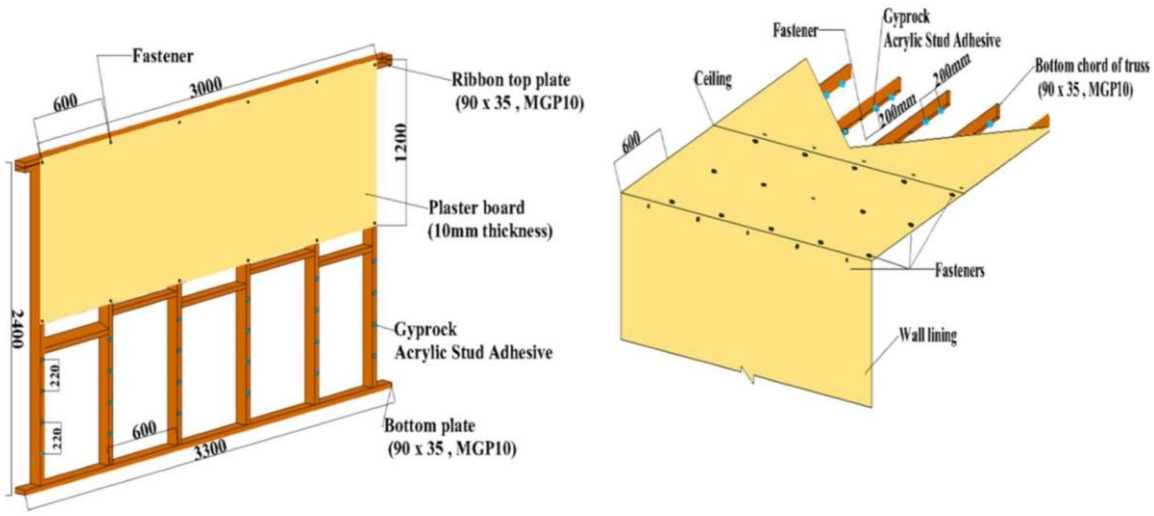

Figure 1-1: LFWS Shear Wall and Roof Structural Details (Satheeskumar et al., 2017)

To address the lack of knowledge about the nonlinear structural behaviour of 3D LFWS buildings, the author was motivated to develop a high-resolution model that simulates every single component of a LFWS building including frames, sheathing panels, and nails. The high-resolution model is used to assess the typical method of design based on hand calculation in terms of being unsafe or overconservative.

The long period of time consumed in the modelling and analysis process of the high-resolution 3D model indicated that high-resolution FEM needs extensive efforts, thus is not anticipated to be used by industrial engineers. This further motivated the author to develop an accurate and efficient alternative simplified FEM for 3D LFWS buildings, so that industrial engineers can conduct the design of 3D LFWS buildings in a faster way.

1.2 Background

Attempts have been made by researchers regarding both high-resolution FEM and simplified FEM of LFWSs at both single wall level and 3D entire building level. A review of the literature related to these approaches is provided below.

1.2.1 High-resolution FEM of LFWS single shear walls

Modelling frame members and sheathing panels as linear isotropic beam elements and shell elements, respectively, have been widely adopted by researchers. Collins et al. (2005a) modelled frame members as isotropic beam elements. Each node of the elements was assigned with three degrees-of-freedoms (DOFs), while each sheathing panel was modelled as a single-layered shell element. Xu and Dolan (2009b) developed a high-resolution shear wall model with isotropic beam elements for frame members and orthotropic shell elements for the OSB sheathing panels. Different moduli of elasticity were assigned to the shell elements in each of the two perpendicular in-plane directions and the out-of-plane directions. Pfretzschner et al. (2014) modelled frame members as isotropic frame elements using commercial software SAP2000 (CSI, 2016). Side-by-side members were treated as a single member, with the area calculated by summing the areas of all of the individual members. Shear walls sheathed with plywood were modelled as orthotropic shell elements, which were assigned both in-plane and out-of-plane properties.

The modelling of sheathing panel nails was treated differently by various researchers, and it is the primary focus of the high-resolution FEM of LFWSs. The sheathing panel nails govern the behaviour of the LFWSs. The majority of the nonlinearity of the LFWSs are captured by the sheathing nails. As such, substantial research has been performed to establish the parametric hysteretic models for the sheathing panel nails. Such hysteretic models or individual fastener tests form the basis of the FEM for the sheathing panel nails. Stewart (1987) proposed a Wayne Stewart hysteresis rule, incorporated nine independent physical parameters. The determination of these parameters is either based on the in-house program CASHEW (Folz and Filiatrault, 2000), or based on experimental data. Baber and Wen (1981) and Baber and Noori (1985) developed a hysteresis model of sheathing fasteners called Bouc-Wen-Baber-Noori (BWBN), which has the capabilities of representing the hardening or softening effect, stiffness and strength degradation, as a function of hysteretic energy dissipation and pinching. The BWBN model (Baber and Noori, 1985; Baber and Wen, 1981) was modified by Xu and Dolan (2009b) so that it can relate the stiffness/strength degradation and pinching behaviour to peak joint

displacement rather than to dissipated energy. The benefit of this modification is to take into consideration the pinching lag phenomenon and small loop simulation, which was eliminated by the BWBN model. Humbert et al. (2014) developed a new constitutive law for the sheathing panel nails that is capable of accurately capturing the hysteretic behaviour of sheathing panel nails by conducting more than 300 experimental tests.

1.2.2 High-resolution FEM of three-dimensional LFWS buildings

A few studies mentioned in Section 1.2.1 have been extended to conduct three-dimensional modelling of LFWS buildings. Collins et al. (2005a) developed a nonlinear FEM procedure for a 3D one-storey LFWS residential building. Each shear wall was modelled using beam elements, shell elements, and two energetically equivalent diagonal nonlinear springs. A series of this kind of shear walls forms a 3D model. The load transferred to each shear wall of the 3D model was calculated, and then a high-resolution FEM was proposed to study the actual response of each shear wall by applying this load. Both the sheathing panels and the frame members in this more high-resolution single-wall model were simulated as shell elements. The sheathing panels-frame members nails were modelled as zero length springs. The accuracy of this three-dimensional nonlinear FEM procedure was verified in the companion paper (Collins et al., 2005b).

A 3D FEM procedure of an entire house with shear walls and diaphragms was proposed by Satheeskumar et al. (2017) using ABAQUS (Smith, 2009) to study the load sharing mechanism under wind loads. Isotropic brick elements and isotropic shell elements were used to model the frame members and sheathing panels of the shear walls, respectively. The sheathing panel-frame member connection was represented by three nonlinear spring elements with the properties obtained from experimental tests of the connections. Frame-to-frame connections were assumed to be surface-to-surface tie constraints. This FEM procedure was verified based on the full-scale test conducted by Satheeskumar et al. (2016), which showed good agreement with the FEM results.

1.2.3 Simplified FEM of LFWS single shear walls

Numerous simplified FEM studies were proposed to avoid the complexity of high-resolution FEM. The use of lateral or diagonal springs are common in the simplified

FEM methods. The properties of these springs are derived either fitting with experimental test or high-resolution FEM analysis results with respect to load-displacement. Gu and Lam (2004) and Xu and Dolan (2009a) stated that the load-deformation behaviour of a fastener in terms of initial linear stiffness, ductility, deformability, strength degradation, and stiffness degradation is similar to that of a shear wall. As such, they stated that the hysteresis law proposed for fasteners can be applied for developing equivalent shear wall models with some modifications. Gu and Lam (2004) related the HYST hysteresis model (Foschi, 2000) of a single nail to the load-displacement response of a shear wall by establishing seven parameters which can be obtained based on the minimum sum of squared error approach. Li et al. (2012) further developed a simplified FEM procedure. The shear walls were modelled with vertical beam elements and diagonal spring elements. Diagonal spring properties were altered from the HYST model (Foschi, 2000). Xu and Dolan (2009a) proposed a simplified FEM method by further modifying the BWBN model (Baber and Noori, 1985; Baber and Wen, 1981) for sheathing panel fasteners in order to simulate an entire shear wall so that the repetitive estimation of the hysteresis of each sheathing panel fastener as mentioned in their other high-resolution modelling method (Xu and Dolan, 2009b) can be avoided. In this simplified FEM, one vertical spring connecting the top plate and the bottom plate is first analyzed in order to obtain the parameters of the BWBN model (Baber and Noori, 1985; Baber and Wen, 1981). The vertical springs in the simplified model is then replaced by two diagonal springs so that the uplift effect can be included, and the parameters obtained from the BWBN model are then adjusted to take into consideration of the uplift effect. Boudaud et al. (2015) developed a simplified FEM method by replacing each high-resolution shear wall with a frame of bars and two-node spring elements. The nonlinear properties of the spring elements were obtained from the constitutive law developed by Humbert et al. (2014) based on the pushover and the cyclic analysis in the corresponding high-resolution models. Chen et al. (2014) developed a similar simplified FEM procedure based on the modification of the BWBN law (Baber and Noori, 1985; Baber and Wen, 1981) and the application of it to the diagonal springs.

Some analytical or mathematical models were also proposed by deriving the stiffness equation for each lateral displacement component. Casagrande et al. (2016) stated that the

lateral displacement of a LFWS shear wall arises from four sources: rigid body rotation, rigid body translation, sheathing-to-framing fastener slip, and shear deformation of the sheathing panels. The load-displacement equation for each individual source was derived by them. Springs were used in the single-storey simplified model "UNITN" to simulate such a load-displacement relationship for each component. Rossi et al. (2016) extended the single-storey UNITN model (Casagrande et al., 2016) to a multi-storey simplified shear wall model. The multi-storey simplified shear wall model was proven to be capable of conducting static and dynamic seismic analysis.

1.2.4 Simplified FEM of three-dimensional LFWS buildings

Tarabia and Itani (1997) proposed a 3D simplified building model with diaphragms and inter-component connection elements only. A shear wall was represented by only one diaphragm. Diaphragms representing the shear walls were connected to the diaphragm representing the floor by inter-component connections. Filiatrault and Folz (2003) proposed a simplified 3D two-storey model called Pancake Model. In this simplified model, the floor diaphragms were modelled as rigid plane stress quadrilateral elements. At the exterior of the diaphragms were frame elements with high axial stiffness and very small bending stiffness. Shear walls were simulated by zero-length nonlinear shear spring elements, and these shear spring elements connected the adjacent floor diaphragms to form a system. The properties of these shear spring elements came from the Wayne Stewart hysteresis rule (Stewart, 1987). Xu and Dolan (2009a) expressed a single shear wall with a top plate, a bottom plate, and a pair of diagonal springs connecting the top plate and the bottom plate. The springs' hysteretic properties were determined from BWBN (Baber and Noori, 1985; Baber and Wen, 1981) single nail model, where thirteen parameters were required to be determined. A 3D two-storey house incorporating eight simplified shear walls and floor diaphragms was modelled. The diaphragms were modelled using shell elements, and their in-plane stiffness were calibrated from quasi-static test. The fundamental period and the seismic time-history analysis result of this simplified 3D model showed good agreement with the experiment (Fischer et al., 2001).

The shear-bending model developed by Pei and van de Lindt (2009) was extended by Pei and van de Lindt (2011) to model a six-storey LFWS building. The rigid plate elements

were adopted for modelling the floor diaphragms. Nonlinear springs elements simulating the shear walls connected the adjacent floor diaphragms to form a system. The hysteresis of the nonlinear springs were estimated from the hysteretic model developed by Folz and Filiatrault (2001). Li et al. (2012) developed a simplified FEM model called PB3D. The floor and roof diaphragms were modelled as combined beam and diagonal truss elements in the simplified FEM model. The in-plane stiffness of the diaphragms that are determined from individual diaphragm test can be simulated by the truss elements. The shear walls were calibrated by vertical beam elements and diagonal spring elements. The spring elements' properties were revised from the HYST model (Foschi, 2000). Martin et al. (2011) simplified the high-resolution FEM by not modelling the individual fasteners, instead, the effect of fasteners was incorporated into sheathing panels by changing the panels' shear modulus. The sheathing panels and the frame members were modelled as a continuous orthotropic thick-shell element with generated auto-meshing, and isotropic beam elements, respectively. Hafeez et al. (2019) established a linear 3D simplified model using rigid frame skeletons and a horizontal spring to simulate each shear wall. The first three components of the single-storey shear wall displacement equation in Canadian timber design standard CSA-O86 (2014) were used to develop the properties of the spring, which accounts for the wall bending, panel shear, and nail slip. respectively. This 3D simplified linear model has the capability of capturing the natural period.

Based on the study of different sources of the lateral displacement of the LFWS buildings, some simplified analytical models for single- and multi-storey LFWS buildings were also proposed. Tomasi et al. (2015) analyzed a three-storey LFWS building using the analytical approach developed by Casagrande et al. (2012). Tomasi et al. (2015) assigned each floor diaphragm with a horizontal constraint. Floor mass was applied in the center of the corresponding diaphragm. The wall stiffness for each component of the lateral displacement (i.e., sheathing panel shear deformation, shear deformation of nails on the sheathing panels, rigid body translation, and rigid body rotation) was expressed, and different springs were adopted to capture the stiffness with respect to the load-displacement relationships.

1.3 Objective of the study

Current structural design of LFWS buildings in industry is based on hand-calculation of individual subassembly. Researchers have been persistently developing tools to conduct computer-aided design using numerical and analytical methods. However, current researches related to the LFWS buildings have two limitations: 1) a few of the high-resolution modelling methods were proven to be capable of analyzing 3D multi-storey LFWS buildings, for this reason, the accurate structural response with the consideration of system effect of the LFWS buildings cannot be captured; 2) some simplified modelling methods for single wall, and single- and multi-storey buildings were developed to reduce the complexity of high-resolution modelling methods, however, numerous parameters need to be determined to obtain the properties of the springs used in the simplified model, which is not practical for industrial engineers. Accordingly, the objectives of the current study are summarized as follows:

1. Propose a simplified nonlinear numerical model for 3D multi-storey LFWS buildings to aid engineers to do structural design of LFWS buildings efficiently.
2. Develop a high-resolution 3D multi-storey numerical model for an actual LFWS building and validate its accuracy through a field measurement.
3. Assess the structural performance (i.e., nonlinearity of the nails and the demand-to-capacity ratios of the frame members and the sheathing panels) of the LFWS building under design loads.
4. Analyze the effect of aspect ratio, tie rod, and gravity load on the stiffness and strength of a shear wall.

1.4 Thesis structure

This thesis has been prepared in the integrated article format. The current chapter introduces the motivation of this topic, along with previous studies related to the high-resolution modelling and simplified modelling method of LFWSs at both single-wall level and 3D building level. The primary objectives of the research are then addressed in subsequent chapters. The final chapter provides a summary of the research and some key findings, followed by a summary of future work related to this research.

1.4.1 Simplified numerical approach for the lateral load analysis of light-frame wood shear wall structures

Chapter two first elaborates the topic of LFWSs with more details explaining the structural components of the LFWSs. A high-resolution FEM method adopted in this research is outlined. Followed by the primary emphasis of this chapter, which is the step-by-step explanation of the proposed simplified FEM for single-storey LFWSs. Six single-storey shear walls with varied wall aspect ratios, tie rods and gravity loads are modelled using both the high-resolution FEM and the simplified FEM for the validation of the simplified FEM procedure. Effects of the variables on the structural performance in terms of stiffness and strength of the LFWSs are then investigated. The simplified FEM procedure is then extended to multi-storey LFWSs. The validation of this multi-storey simplified numerical approach is conducted in the end with the consideration of four multi-storey shear walls with different aspect ratios and tie rods.

1.4.2 High-resolution and simplified numerical modelling of a four-storey light-frame wood building

Chapter three further extends both the high-resolution FEM and the simplified FEM discussed in Chapter two to 3D multi-storey LFWS buildings. A case study of an actual 3D four-storey LFWS building recently completed in Ontario, Canada, is performed in this chapter. The structural details of the case-studied building are described in the beginning. The high-resolution FEM method for this building is then demonstrated with details. The building natural frequencies obtained from the field test are then compared with the natural frequencies analyzed from the high-resolution model's modal analysis. Then, the simplified FEM is applied to this building. The comparison of the pushover analyses of both the high-resolution and the simplified 3D four-storey building models is performed to validate the accuracy of the simplified model. In the end, the validated high-resolution model is used to study the structural performance under design loads.

1.5 References

Baber, T. T., & Noori, M. N. (1985). Random vibration of degrading, pinching systems. *Journal of the Engineering Mechanics Division*, *111*(8), 1010–1026. https://doi.org/10.1061/(ASCE)0733-9399(1985)111:8(1010)

Baber, T. T., & Wen, Y.-K. (1981). Random Vibration Hysteretic, Degrading Systems. *Journal of the Engineering Mechanics Division*, *107*(6), 1069–1087.

Boudaud, C., Humbert, J., Baroth, J., Hameury, S., & Daudeville, L. (2015). Joints and wood shear walls modelling II: Experimental tests and FE models under seismic loading. *Engineering Structures*, *101*, 743–749. https://doi.org/10.1016/j.engstruct.2014.10.053

Casagrande, D., Rossi, S., Sartori, T., & Tomasi, R. (2012). Analytical and numerical analysis of timber framed shear walls. *World Conference on Timber Engineering 2012*.

Casagrande, D., Rossi, S., Sartori, T., & Tomasi, R. (2016). Proposal of an analytical procedure and a simplified numerical model for elastic response of single-storey timber shear-walls. *Construction and Building Materials*, *102*, 1101–1112. https://doi.org/10.1016/j.conbuildmat.2014.12.114

Chen, Z., Chui, Y. H., Ni, C., Mohammad, M., & Doudak, G. (2014). Simulation of the lateral drift of multi-storey light wood frame buildings based on a modified macro-element model. *WCTE 2014 - World Conference on Timber Engineering*, 1–9. Quebec City, Canada.

Collins, M., Kasal, B., Paevere, P., & Foliente, G. C. (2005a). Three-Dimensional Model of Light Frame Wood Buildings. I: Model Description. *Journal of Structural Engineering*, *131*(4), 676–683. https://doi.org/10.1061/(ASCE)0733-9445(2005)131

Collins, M., Kasal, B., Paevere, P., & Foliente, G. C. (2005b). Three-dimensional model of light frame wood buildings. II: Experimental investigation and validation of analytical model. *Journal of Structural Engineering*, *131*(4), 684–692. https://doi.org/10.1061/(ASCE)0733-9445(2005)131:4(684)

CSA-O86. (2014). Engineering Design in Wood. In *Canadian Standards Association*. Retrieved from http://shop.csa.ca/en/canada/structures/o86-09-consolidation/invt/27013742009

CSI. (2016). Analysis Reference Manual for SAP2000, ETABS, SAFE and CSiBridge. In *Computers and Structures, Inc.* Retrieved from http://docs.csiamerica.com/manuals/etabs/Analysis Reference.pdf

Filiatrault, A., Isoda, H., & Folz, B. (2003). Hysteretic damping of wood framed buildings. *Engineering Structures*, *25*(4), 461–471. https://doi.org/10.1016/S0141-0296(02)00187-6

Fischer, D., Filiatrault, A., Folz, B., Uang, C.-M., & Seible, F. (2001). Shake Table Tests of a Two-Story Woodframe House. In *CUREE No. W-06*. Richmond, California, USA.

Folz, B., & Filiatrault, A. (2000). CASHEW - Version 1.0: A computer program for cyclic analysis of wood shear walls. In *Management*.

Folz, B., & Filiatrault, A. (2001). Cyclic analysis of wood shear walls. *Journal of Structural Engineering*, *127*(4), 433–441. https://doi.org/10.1061/(ASCE)0733-9445(2001)127:4(433)

Foschi, R. O. (2000). Modeling the hysteretic response of mechanical connections for wood structures. *6th World Conference on Timber Engineering*, 1–11. Whistler, Canada.

Gu, J. Z., & Lam, F. (2004). Simplified mechanics-based wood frame shear wall model. *13th World Conference on Earthquake Engineering*, 1–11. Vancouver, B.C., Canada.

Hafeez, G., Doudak, G., & McClure, G. (2019). Dynamic characteristics of light-frame wood buildings. *Canadian Journal of Civil Engineering*, *46*(1), 1–12. https://doi.org/10.1139/cjce-2017-0266

Humbert, J., Boudaud, C., Baroth, J., Hameury, S., & Daudeville, L. (2014). Joints and wood shear walls modelling I: Constitutive law, experimental tests and FE model under quasi-static loading. *Engineering Structures*, *65*, 52–61. https://doi.org/10.1016/j.engstruct.2014.01.047

Itani, R. Y., & Cheung, C. K. (1984). Nonlinear analysis of sheathed wood diaphragms. *Journal of Structural Engineering*, *110*(9), 2137–2147.

Kuzman, M. K., & Sandberg, D. (2017). Development of Multi-Storey Timber Buildings and Future Trends. *II Latin American Congress on Timber Structures*, 1–7. Junin, Argentina.

Li, M., Lam, F., Foschi, R. O., Nakajima, S., & Nakagawa, T. (2012). Seismic performance of post and beam timber buildings I: Model development and verification. *Journal of Wood Science*, *58*(1), 20–30. https://doi.org/10.1007/s10086-011-1219-5

Martin, K. G., Gupta, R., Prevatt, D. O., Datin, P. L., & Van De Lindt, J. W. (2011). Modeling system effects and structural load paths in a wood-framed structure. *Journal of Architectural Engineering*, *17*(4), 134–143. https://doi.org/10.1061/(ASCE)AE.1943-5568.0000045

Mi, H. (2004). *Behavior of unblocked wood shear walls* (University of New Brunswick, Fredericton, Canada). Retrieved from http://scholar.google.com/scholar?hl=en&btnG=Search&q=intitle:Behavior+of+unblocked+wood+shearwalls#1

NBCC. (2015). *National Building Code of Canada*. National Research Council of Canada, Ottawa, Canada.

Niazi, M., El Damatty, A., & Hamada, A. (2018). Sensitivity study of the light-framed wood shear walls subjected to lateral loads. *6th International Structural Specialty Conference 2018, Held as Part of the Canadian Society for Civil Engineering Annual Conference 2018*, 1–9. Fredericton, Canada.

Pei, S., & van de Lindt, J. W. (2009). Coupled shear-bending formulation for seismic analysis of stacked wood shear wall systems. *Earthquake Engineering and Structural Dynamics*, *38*(14), 1631–1647. https://doi.org/10.1002/eqe

Pei, S., & van de Lindt, J. W. (2011). Seismic numerical modeling of a six-story light-frame wood building: Comparison with experiments. *Journal of Earthquake Engineering*, *15*(6), 924–941. https://doi.org/10.1080/13632469.2010.544840

Pfretzschner, K. S., Gupta, R., & Miller, T. H. (2014). Practical modeling for wind load paths in a realistic light-frame wood house. *Journal of Performance of Constructed Facilities*, *28*(3), 430–439. https://doi.org/10.1061/(ASCE)CF.1943-5509.0000448

Rossi, S., Casagrande, D., Tomasi, R., & Piazza, M. (2016). Seismic elastic analysis of light timber-frame multi-storey buildings: Proposal of an iterative approach. *Construction and Building Materials*, *102*, 1154–1167. https://doi.org/10.1016/j.conbuildmat.2015.09.037

Satheeskumar, N., Henderson, D. J., Ginger, J. D., Humphreys, M. T., & Wang, C. H. (2016). Load sharing and structural response of roof–wall system in a timber-framed house. *Engineering Structures*, *122*, 310–322. https://doi.org/10.1016/j.engstruct.2016.05.009

Satheeskumar, Navaratnam, Henderson, D. J., Ginger, J. D., & Wang, C. H. (2017). Three-Dimensional Finite-Element Modeling and Validation of a Timber-Framed House to Wind Loading. *Journal of Structural Engineering (United States)*, *143*(9). https://doi.org/10.1061/(ASCE)ST.1943-541X.0001850

Smith, S. (2009). *ABAQUS Standard User's Manual, Version 6.9*. Providence, RI.

Stewart, W. G. (1987). *The seismic design of plywood sheathed shear walls*. University of Canterbury, Christchurch, New Zealand.

Tarabia, A. M., & Itani, R. Y. (1997). Static and dynamic modeling of light-frame wood buildings. *Computers & Structures*, *63*(2), 319–334.

Tomasi, R., Sartori, T., Casagrande, D., & Piazza, M. (2015). Shaking table testing of a full-scale prefabricated three-story timber-frame building. *Journal of Earthquake Engineering*, *19*(3), 505–534. https://doi.org/10.1080/13632469.2014.974291

Winkel, M. H. (2006). Behavior of light-frame walls subject to combined in-plane and out of plane loads (University of New Brunswick, Fredericton, Canada). Retrieved from http://scholar.google.com/scholar?hl=en&btnG=Search&q=intitle:Behavior+of+light-frame+walls+subject+to+combined+in-plane+and+out+of+plane+loads#0

Winkel, M., & Smith, I. (2010). Structural behavior of wood light-frame wall segments subjected to in-plane and out-of-plane forces. *Journal of Structural Engineering*, *136*(7), 826–836. https://doi.org/10.1061/(ASCE)ST.1943-541X.0000170

Xu, J., & Dolan, J. D. (2009a). Development of a wood-frame shear wall model in ABAQUS. *Journal of Structural Engineering*, *135*(8), 977–984. https://doi.org/10.1061/(ASCE)ST.1943-541X.0000031

Xu, J., & Dolan, J. D. (2009b). Development of nailed wood joint element in ABAQUS. *Journal of Structural Engineering*, *135*(8), 968–976. https://doi.org/10.1061/(ASCE)ST.1943-541X.0000030

Chapter 2

2 Simplified Numerical Approach for the Lateral Load Analysis of Light-Frame Wood Shear Wall Structures

2.1 Introduction

As one of the world's oldest construction materials, wood has played an important role in human endeavours. Up to the 19th century, wood was the most important raw material for all types of construction (Kuzman and Sandberg, 2017). However, due to the deficiency of wood with respect to fire resistance and the increasing demand for high-rise buildings, concrete and steel were later substituted for wood. Today, because wood is durable, easy to use for construction, recyclable, and sustainable, wooden structural systems have reclaimed global attention. The development of fire-retardant materials and design procedures, such as standard time-temperature exposure methods and performance-based fire design principles, has gradually addressed obstacles related to fire safely. Researchers and engineers are also diligently promoting the construction of higher and higher timber structures. The National Building Code of Canada (NBCC, 2015) allows up to six storeys of wood-frame structures, an increase from the previous code provision that limited wood-frame structures to four storeys. There are two types of wood-frame structures: LFWSs and heavy timber structures. The weaker strength and lower fire resistance rating of high-rise LFWSs have resulted in the much slower proliferation of these buildings compared to that of high-rise heavy timber structures. However, LFWSs offer lower cost and superior seismic response performance because the nonlinearity of their numerous fasteners enables them to absorb tremendous energy. These benefits have created a greater demand for higher LFWSs and have provided the motivation for this study: to develop a more effective FEM method for modelling and analyzing LFWSs in a way that will enable the efficient study of their behaviour under lateral loads, which represents an essential step forward in high rise LFWS research.

A LFWS is typically composed of frame, sheathing panels, fasteners, and anchorage (Figure 2-1). The framing comprises precast dimension lumber, usually 38 mm × 89 mm or 38 mm × 140 mm. Dimension lumber aligned in a vertical direction functions as a

column but is called a stud. The two end studs are called end posts. Studs are usually spaced 610 mm, 406 mm, and 305 mm apart, depending on the magnitude of the gravity load. Dimension lumber positioned in a horizontal direction performs like a beam, but in a timber structure, such elements are called the top plate, the blocking, and the bottom plate. The top plate can be either a single- or a double-layered structure, but the most common type is a double top plate, which refers to two layers of dimension lumber nailed together with little or no offset. The top plate provides the strength needed for transferring the loading from the floor joists to the studs. Blocking is used at the exterior edges of sheathing panels, usually at the midpoint or at 1/3 and 2/3 of the height of a shear wall. Blocking prevents the studs from buckling, provides support for the sheathing panels, and also contributes additional lateral resistance. The bottom plate, which usually has a single layer bolted or nailed to the lower storey, transfers the load uniformly from the studs to the lower storey. A hold-down or tie rod is normally anchored to the ground on two ends of a shear wall. A hold-down can provide both axial and shear resistance, but a tie rod is a tension-only bar. In a tie rod system, the take-up device is supported by a top plate that connects two steel rods above and below the top plate. This configuration enables the tension force of the upper-storey tie rod to be transferred to the lower storeys, and the tension force accumulated on the lowest storey tie rod then to be transferred to the ground.

A sheathing panel is usually 1220 mm × 2440 mm. Sheathing panels are nailed to the frame on either one or both sides of the frame. Sheathing panels can be either plywood or oriented strand board (OSB). A sheathing panel is the main system for resisting lateral force, and external wall sheathing panels can also function as a component of the building envelope. Some walls are also sheathed with gypsum wall board (GWB) in order to provide fire resistance. The only GWB product permitted according to the Canadian timber design standard (CSA-O86, 2014) is 15.9 mm Type X GWB. The fasteners (nails) used in a shear wall are either framing-to-framing (FF) or sheathing-to-framing (SF) nails. FF nails connect the two top plate layers and fasten the plate to the studs. SF nails are usually placed with compact spacing at panel edges and with less dense spacing at interior panels. The nails constitute the primary source of the nonlinearity of a shear wall system, dissipating a great deal of energy during an earthquake event.

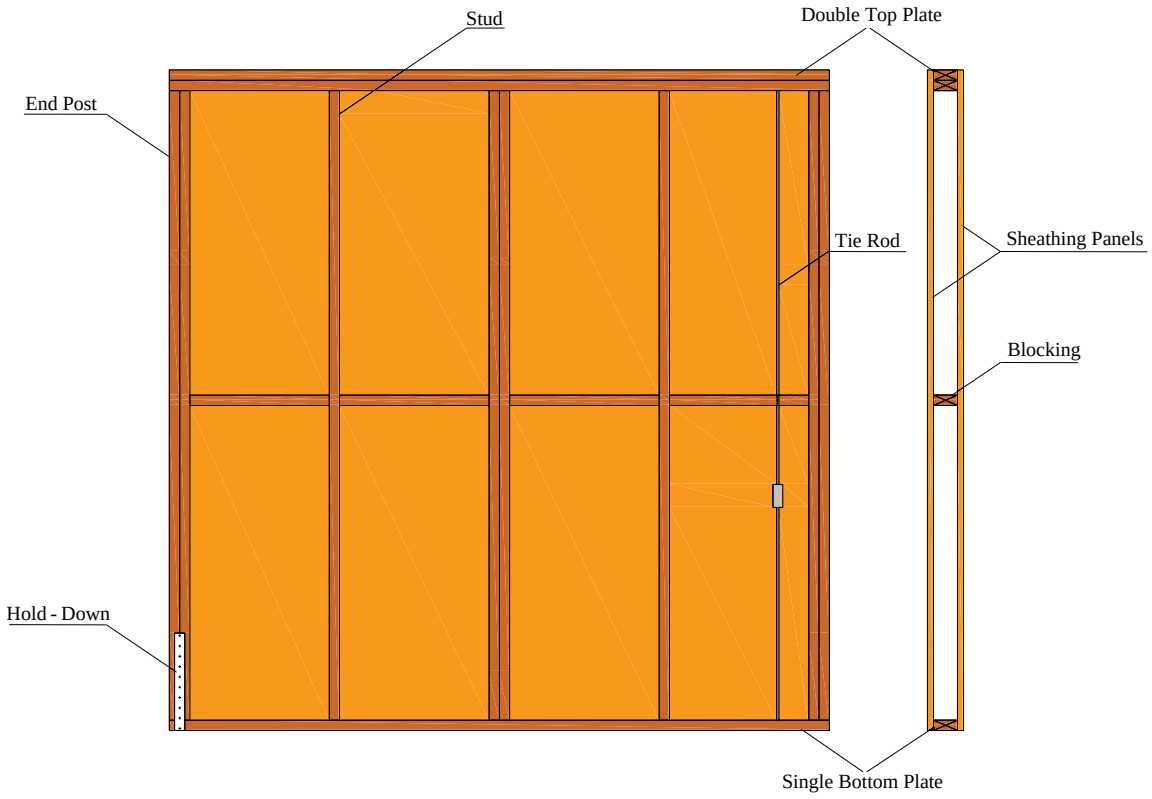

Figure 2-1: Common components of a LFWS

Studies related to the numerical modelling of LFWSs can be divided into high-resolution FEM and simplified FEM. A review of the literature related to both approaches is provided below. Broad consensus has been reached with respect to high-resolution FEM modelling of framing members as linear isotropic beam elements and of sheathing panels as shell elements. Pfretzschner et al. (2014) assigned an isotropic frame element to each framing member using commercial software SAP2000 (CSI, 2016), with side-by-side members modelled as a single member with the area equal to the sum of the areas of all of the individual members. Plywood wall sheathings were modelled as orthotropic shell elements with both in-plane and out-of-plane properties. Xu and Dolan (2009b) established a high-resolution shear wall model in which the framing members were modelled as isotropic beam elements and the OSB sheathing panels as orthotropic shell elements with different modulus of elasticity in each direction. Collins et al. (2005a) modelled framing members as isotropic beam elements with three DOFs per node and each sheathing panel as a single-layered shell element.

A primary focus of LFWS research has been the modelling of sheathing fasteners (SF nails) in high-resolution FEM, which has differed from researcher to researcher. SF fasteners constitute the main source of LFWSs nonlinearity, and their behaviour governs the LFWSs response. For this reason, substantial research has been conducted with the goal of establishing a parametric hysteretic model for fasteners. FEM for fasteners is usually based on such hysteretic models or on individual fastener tests. Baber and Wen (1981) and Baber and Noori (1985) developed a hysteresis model of sheathing fasteners called Bouc-Wen-Baber-Noori (BWBN), which is capable of representing the hardening or softening effect, stiffness and strength degradation, as a function of hysteretic energy dissipation and pinching. Xu and Dolan (2009b) modified the BWBN model (Baber and Noori, 1985; Baber and Wen, 1981) so that it relates the stiffness/strength degradation and pinching behavior to peak joint displacement rather than to dissipated energy, which eliminates the pinching lag phenomenon and small loop simulation. The Wayne Stewart hysteresis rule proposed by Stewart (Stewart, 1987) incorporates nine independent physical parameters, which can be determined either from the in-house program CASHEW (Folz and Filiatrault, 2000), or from experimental data. Humbert et al. (2014) developed a new sheathing fastener constitutive law capable of accurately describing the hysteretic behaviour of FF and SF nails based on more than 300 experimental tests.

High-resolution FEM consumes a substantial amount of time for both the modelling process and analysis, particularly for dynamic analysis. This deficiency is likely attributable to the following factors: 1) multiple two-node spring-like nonlinear connections (SF, FF, wall-to-floor/roof and wall-to-foundation), with each node having three DOFs; 2) the fact that each sheathing panel is meshed into multiple four-node elements based on nail distance and that every node of the meshed elements has three DOFs. This inefficiency limits the efficacy of the high-resolution modelling method for both academic and industry applications.

Numerous studies have further substituted an energetically equivalent simplified method for a high-resolution FEM model. The most common simplified method is based on the use of lateral or diagonal springs, whose hysteresis properties are derived from fitting in experimental or high-resolution FEM load-displacement analysis results. Gu and Lam

(2004) and Xu and Dolan (2009a) state that the load-deformation behaviour of a shear wall resembles that of a fastener with respect to initial linear stiffness, ductility, deformability, strength degradation, and stiffness degradation. With some modifications, the hysteresis law proposed for fasteners can therefore be applied for establishing equivalent shear wall models. Gu and Lam (2004) related a single-nail hysteresis HYST model proposed by Foschi (2000) to the load-displacement response of two shear walls by establishing seven parameters resulting from different search methods based on the minimum sum of squared error approach. Li et al. (2012) conducted a further simplified FEM analysis by modelling shear walls with vertical beam elements and diagonal spring elements. They altered the HYST model (Foschi, 2000) to establish the diagonal spring properties. Xu and Dolan (2009a) introduced additional modifications to the BWBN model (Baber and Noori, 1985; Baber and Wen, 1981) in order to simulate an entire shear wall while avoiding the repetitive estimation of the hysteresis of each sheathing fastener required with their other high-resolution modelling method (Xu and Dolan, 2009b). With their modified technique, one spring connecting the top and bottom plates is first analyzed in order to examine the BWBN model (Baber and Noori, 1985; Baber and Wen, 1981) parameters. These parameters are then adjusted to allow for the uplift effect created by the use of two diagonal springs. In a companion paper to the one published by Humbert et al. (2014), Boudaud et al. (2015) simplified each single shear wall with a frame of bars and two-node spring elements. The nonlinear properties of the spring elements were based on the constitutive law as described by Humbert et al. (2014), and the parameters of the constitutive law were obtained from high-resolution model pushover and cyclic analysis. Chen et al. (2014) conducted a similar simplified analysis by modifying the BWBN law (Baber and Noori, 1985; Baber and Wen, 1981) and applying it to a diagonal spring.

Another category of simplified method is based on the analytical or mathematical derivation of each lateral displacement component. Casagrande et al. (2016) classified lateral displacement as arising from four sources: rigid body rotation, rigid body translation, SF nails slip, and shear deformation of the sheathing panels. They generated load-displacement equation for each individual source, and three springs were used in a simplified single-storey model called UNITN as a means of simulating such a load-

displacement relationship. Rossi et al. (2016) replicated the single-storey UNITN model (Casagrande et al., 2016) for a multi-storey shear wall model, which is capable of conducting static and dynamic seismic analysis.

For the following reasons, previously developed simplified FEM are still insufficient: 1) Only a few of the simplified models (Chen et al., 2014; Li et al., 2012; Rossi et al., 2016; Xu and Dolan, 2009a) have been applied to a multi-storey shear wall structure in order to verify their accuracy. 2) Either numerous parameters of the simplified spring hysteresis relationship must be determined for it to fit into the experimental or high-resolution FEM analysis results, or, with analytical and mathematical simplified methods, the requirement to conduct many complex calculation processes makes them impractical for easy application in the design industry. 3) The imperfect validation of simplified FEM pushover analysis means that errors could accumulate when even higher multi-storey LFWSs are analyzed. An efficient and accurate simplified FEM for use with multi-storey LFWSs is therefore urgently needed.

This chapter is structured as follows. The high-resolution FEM procedure adopted is first presented in depth, followed by the introduction and step-by-step explanation of a proposed simplified FEM, called a two-link model. The next section validates this simplified FEM procedure through the use of both high-resolution and simplified FEM for the pushover analysis of six single-storey shear walls characterized by varied aspect ratios, tie rods, and gravity loads. The final section describes the evolution and replication of the single-storey simplified FEM in order to form a multi-storey simplified FEM, and also details the validation of this new multi-storey simplified FEM.

2.2 Overview of the adopted FEM modelling procedure

The single-shear-wall numerical FEM procedure proposed by Niazi et al. (2018) was employed for this study. The model developed using the commercial software ETABS (CSI, 2016) considered all of the wall components, including studs, plates, blocking, sheathing panels, SF nails, and FF nails. Beam elements and shell elements were used for simulating the frame members (i.e., studs, plates, and blocking) and the sheathing panels, respectively. A two-node link element was employed for the simulation of the SF and FF

nails. The frame elements and shell elements were meshed manually based on the nail spacing at the edges of the sheathing panels. Niazi et al. (2018) performed pushover analysis on a FEM model whose prototype was monotonically tested by Winkel and Smith (2010). For their study, the dimension of the test specimen was 2440 mm × 2440 mm. Five 38 mm × 89 mm studs were uniformly distributed along the length of the shear wall, and the studs and plates were sheathed on one side using nails and sheathing panels that are 11.1 mm thick. The shear wall was fixed to the steel base by four anchor bolts. Two identical sets of this specimen were tested by subjecting them to the same racking load, but different initial stiffness and ductility test results were obtained from the experiments. Winkel and Smith (2010) did not explicitly explain why different results were obtained from the experiment even though the test specimens were the same, and why there was a sudden brittle failure at the second test. The strength and ductility values produced by the numerical analysis matched well with the first experimental test results, and the initial stiffness computed by the numerical analysis matched well with that from the second test results. In general, the pushover analysis result showed reasonably good agreement with the experimental findings. Details of the shear wall FEM model and a comparison of its result with the experimental findings are shown in Figure 2-2.

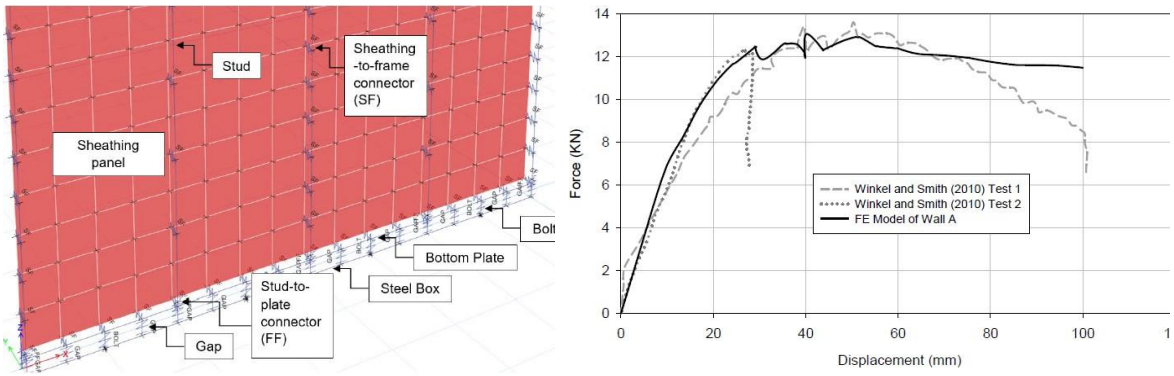

(a) Single shear wall FEM model details (b) Comparison with test

Figure 2-2: (a) Shear wall high-resolution FEM model details and (b) its pushover result compared with the experimental findings (Niazi et al., 2018)

2.3 Simplified modelling procedure

The high-resolution FEM procedure mentioned above requires extensive effort for the modelling and analysis because it takes into account all of the shear wall components. This feature makes it impractical for both academic and industrial applications. A need therefore exists for the development of a simple and efficient alternative for modelling multi-storey LFWS that yields accurate results in terms of initial stiffness, peak load, and ductility. The work conducted for the study presented here resulted in the proposal of a two-link model (Figure 2-3). The two side-links have axial and shear stiffness, and the beam element connecting the two side-links is rigid in all directions. This method is capable of incorporating consideration of the effect of the gravitational load F_V on the lateral behaviour of the shear walls. The development of the simplified method starts by considering the load-displacement results from the pushover analysis obtained using the high-resolution model. The displacement is decomposed into flexural and shear displacement, and these two displacement components are applied for transforming the values so that they reflect the axial and shear stiffness values for the two side-links, respectively. The theory underlying this procedure is that the work done by the external load equals the work performed by the internal load.

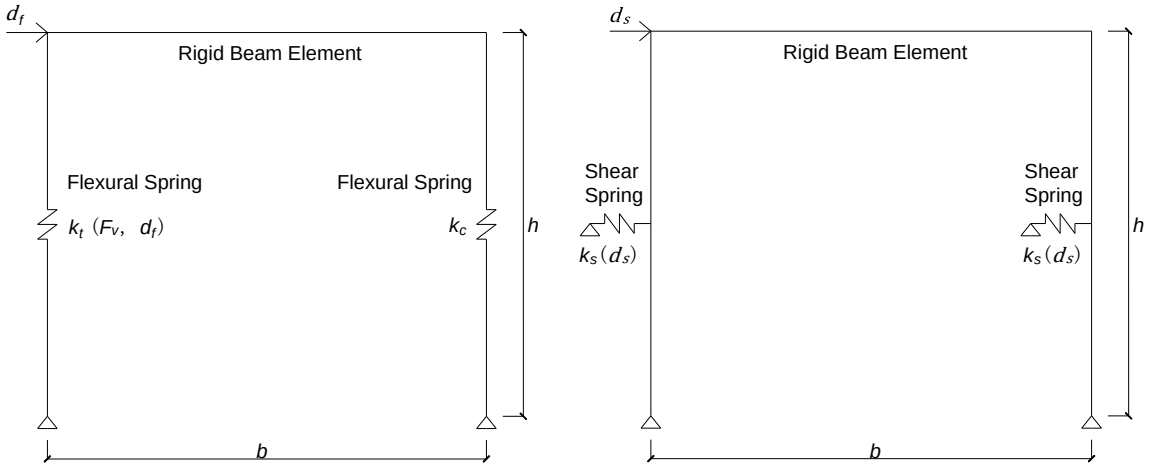

(a) Simplified model flexural springs (b) Simplified model shear springs

Figure 2-3: Simplified "two-link" model: (a) simplified model flexural springs; (b) simplified model shear springs

2.3.1 Modelling procedure

The procedure for obtaining the axial and shear stiffness values for the two side-links is illustrated by the flowchart provided in Figure 2-4. A detailed explanation follows.

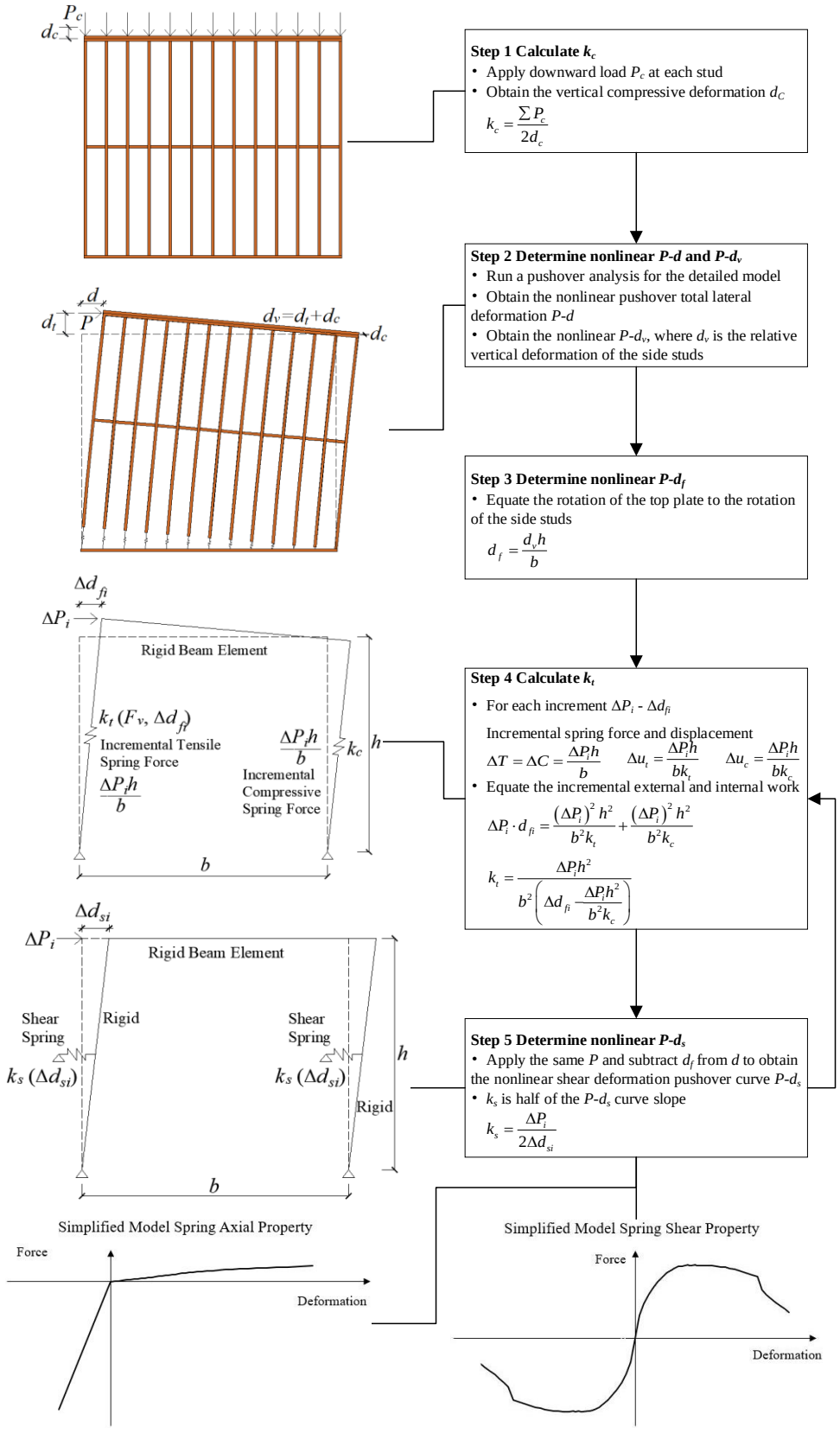

Figure 2-4: Flowchart of the simplified FEM procedure

Step 1: Computation of the equivalent compressive stiffness k_c

The first step in the simplified procedure is the computation of the equivalent compressive stiffness k_c. Downward loads (P_c) are applied at each stud, and a nonlinear analysis is carried out incrementally. The result shows a linear relationship between the applied downward load and the vertical deformation of the wall, which indicates that the compressive stiffness of the wall is constant. The compressive stiffness of the simplified model k_c can be obtained from $\Sigma P_c/(2d_c)$, where ΣP_c is the sum of all downward loads and d_c is the vertical deformation of the wall resulting from the downward load. In the simplified model, both springs have the capacity to resist the compressive force, so a scaler "2" is included in the denominator.

Step 2: Determination of the nonlinear lateral total deformation pushover analysis curve *P-d* and the nonlinear relative vertical deformation versus lateral base shear curve P-d_v

The second step is to conduct pushover analysis using the high-resolution model and to obtain the nonlinear result in the form of base shear (P) versus lateral deformation (d) and base shear (P) versus the relative vertical displacement of the side-studs (d_v). The frame member bending effect is so small that researchers (Casagrande et al., 2016; Filiatrault et al., 2003; Itani and Cheung, 1984) usually ignore it. In the following step, the P-d_v curve acquired from the high-resolution model is transformed in order to obtain P-d_f based on the assumption that the frame members from the high-resolution model have no bending effect, where d_f is the lateral flexural displacement. Next, d_f is transformed in order to compute the simplified model spring tensile stiffness k_t. Subtracting d_f from the total lateral displacement d yields the shear displacement d_s, which is used for calculating the simplified model spring shear stiffness k_s.

Step 3: Determination of the nonlinear flexural deformation curve P-d_f

The nonlinear flexural deformation curve P-d_f is obtained by transforming P-d_v, acquired in Step 2, based on the assumption that the frame members from high-resolution model have no bending effect so that the rotation of the top plate (d_v/b) equals the rotation of

the side studs (d_f/h). The value of d_f can thus be derived from $d_f = (d_v h)/b$, where d_v is taken from Step 2, h is the storey height, and b is the distance between the two vertical side-links, which can be considered equal to the wall width.

Step 4: Computation of the equivalent tensile stiffness k_t

The equivalent tensile stiffness k_t of the link is obtained from the P-d_f curve based on the equating of the incremental external and internal work. Consider an incremental external load ΔP_i (i.e., $P_i - P_{i-1}$) and a corresponding incremental deflection Δd_{fi}. Based on consideration of the equilibrium of moment, the incremental axial loads at the two side-links are $\Delta T = (\Delta P_i h)/b$ and $\Delta C = (\Delta P_i h)/b$, where h is the storey height and b is the wall width. The corresponding incremental displacement values at the tensile spring (Δu_t) and at the compressive spring (Δu_c) are $\Delta u_t = (\Delta P_i h)/(bk_t)$ and $\Delta u_c = (\Delta P_i h)/(bk_c)$, respectively. Equating the incremental external work and the incremental internal work yields the following:

$$\Delta P_i \times d_{fi} = \frac{(\Delta P_i)^2 h^2}{b^2 k_t} + \frac{(\Delta P_i)^2 h^2}{b^2 k_c} \tag{1-1}$$

for which k_t can be calculated as follows:

$$k_t = \frac{\Delta P_i h^2}{b^2\left(\Delta d_{fi} - \frac{\Delta P_i h^2}{b^2 k_c}\right)} \tag{1-2}$$

From the nonlinear curve P-d_f, the incremental load ΔP_i and its corresponding incremental displacement Δd_{fi} can be computed. Knowing the compressive stiffness k_c and the dimensions b and h enables the tensile stiffness k_t to be established. Since the pushover curve P-d_f is nonlinear, k_t will clearly vary nonlinearly with Δd_{fi}.

Step 5: Determination of the nonlinear shear deformation curve P-d_s

After the nonlinear P-d and P-d_f curves have been obtained, the nonlinear shear deformation curve (P-d_s) is derived based on the subtraction of d_f from d at the same lateral load P (Figure 2-5). The simplified model shear stiffness value k_s is half of the

slope of the P-d_s curve ($k_s = \Delta P_i/(2\Delta d_{si})$) because there are two shear springs in parallel. It is also clear that k_s varies nonlinearly because P-d_s is nonlinear.

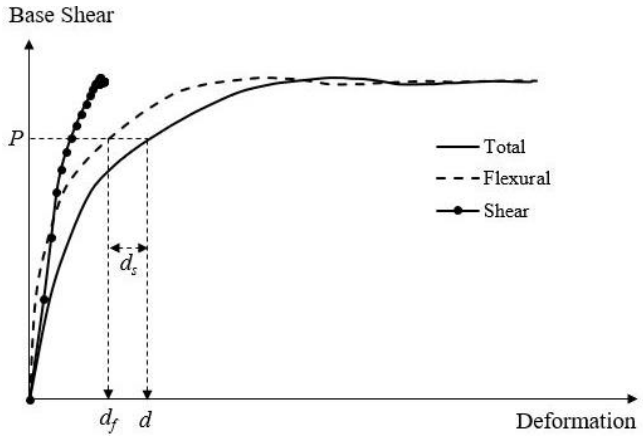

Figure 2-5: Component of the pushover analysis result

The two side-links are modelled on ETABS (CSI, 2016) as multi-linear link elements. The axial and shear properties in the form of nonlinear load-displacement functions must be defined for the link element. Through the repetition of Step 4 and Step 5, a series of varying k_t and k_s values can be obtained. Consequently, the nonlinear load-displacement functions of the link axial and shear properties can be determined. Because the link can resist shear forces coming from both the right and left directions, the load-deformation curve is thus symmetric about the origin.

2.3.2 Effect of the gravity load F_V

When Steps 1 to 5 are applied as outlined in section 2.3.1, the characteristics of the springs k_c, k_t, and k_s can be obtained. It should be mentioned that k_c is linear, while both k_t and k_s are nonlinear. The gravity load F_V also has an influence on the characteristics of k_t. Steps 2 to 4 from section 3.1 can be repeated for different values of F_V in order to establish the corresponding characteristics of k_t.

Combining nonlinear load cases using linear addition is inaccurate. For an accurate nonlinear pushover analysis that incorporates consideration of the gravity load, the ETABS (CSI, 2016) high-resolution model pushover analysis (Step 2 in section 2.3.1) should begin with an initial condition for the calculation of the stress and deformation

from the nonlinear gravity load case. The gravity load represents the sum of both the self-weight of all members (denoted as the default nonlinear "Dead" load case in ETABS (CSI, 2016)) and the vertical load acting on the floor (denoted as the nonlinear "Downward Load" load case in ETABS (CSI, 2016)). The "Downward Load" load case starts from the "Dead" load case, with the "Downward Load" load case then becoming the initial condition of the "Pushover" load case (Figure 2-6). In this way, the loading sequence can also be captured.

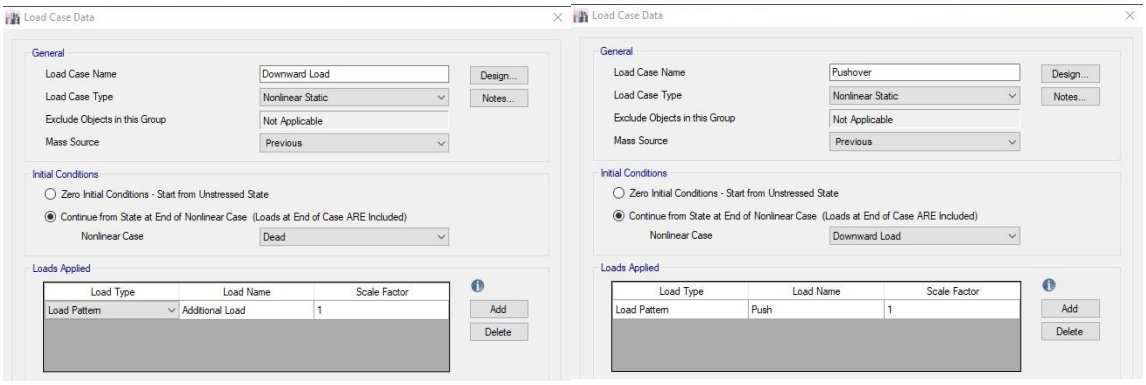

Figure 2-6: Consideration of the gravitational load in ETABS (CSI, 2016)

2.3.3 Effect of the tie rods

Often in LFWS, tie rod systems are added to both ends of the walls as a means of improving the tensile stiffness of the walls and, consequently, their flexural stiffness. To account for the effect of the tie rods, the high-resolution model can include uniaxial bar elements that simulate tie rods. Steps 2 to 5 in section 2.3.1 can then be repeated using the pushover curve (*P-d*) from the high-resolution model that includes the tie rods.

2.4 Simplified modelling for single-storey single walls

2.4.1 Details of the six walls studied

Six high-resolution FEM studies were performed based on varied wall lengths, tie rods, and gravity loads (Table 2-1) in order to examine the effect of changing these factors on the ability of the wall to resist lateral loads and also to obtain the corresponding simplified model link properties to be employed for validating the results produced using the simplified FEM.

The procedure described above was applied to a short and a long shear wall, labelled W_S and W_L, respectively. These two shear walls were selected from a real project recently completed in Ontario, Canada. The short shear wall W_S (Figure 2-7) was 1.22 m wide and 3.19 m high. The framing was sheathed on one side with 11 mm Type 1 OSB sheathing panels having a standard dimension of 1220 mm × 2440 mm. Panels edges were fastened by plates, blocking, and studs with common wire nails 64 mm long, with a diameter of 3.3 mm and spaced 150 mm apart. The interior sheathing was fastened to studs with the same nails spaced 300 mm apart. All wood studs, posts, plates, and blocking were spruce-pine-fir (SPF) 38 mm × 140 mm dimension lumber. Except for the length, which was 3.66 m wide, all other structural details for W_L were the same as for W_S. Other than the self-weight, no additional gravity load was applied on either W_S or W_L.

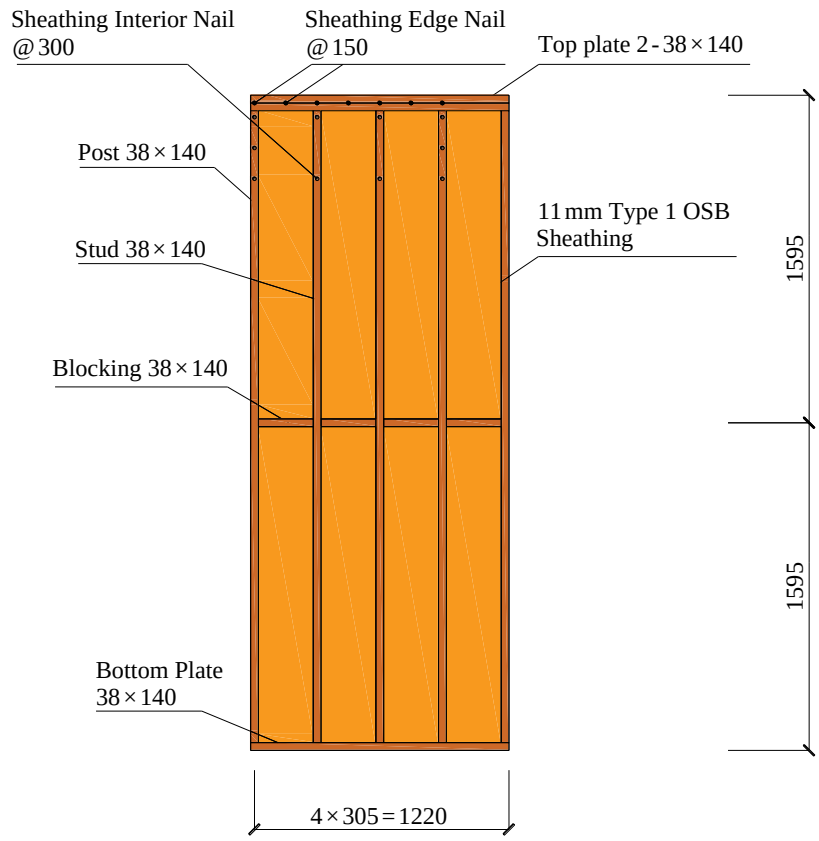

Figure 2-7: Structural details of the W_S shear wall (dimensions: mm)

The simplified procedure was also applied to both of the other types of shear walls labelled W_{ST} and W_{LT}. The only difference between W_{ST} and W_S, or between W_{LT} and W_L, is that W_{ST} and W_{LT} included one Simpson Strong-Tie tie rod (ATS, 2008) at both ends of each wall to increase the tensile stiffness. For this study the tie rod system was composed of a steel rod and a take-up device. The length of each steel rod segment was equal to the storey height, and the steel rod segments were connected by take-up devices supported by the top plates. For both W_{ST} and W_{LT}, the tie rods were simulated as uniaxial bar elements with a stiffness of 233.5 kN/mm calculated based on (ATS, 2008).

The structural details of the last two types of the shear walls studied, labelled W_{SV} and W_{LV}, are the same as those of W_S and W_L, respectively. Unlike W_S and W_L, for which no additional gravity load was applied, distributed gravity loads of 80 kN/m were applied on the top plates of W_{SV} and W_{LV} to represent the dead and live loads of the upper walls and floors. This gravity load was calculated based on consideration of a 5 m tributary width perpendicular to the direction of the wall length. All of the six shear walls studied had the same stud, plate, blocking, sheathing, and nail types and spacing. The varied factors for W_S and W_L, W_{ST} and W_{LT}, and W_{SV} and W_{LV} are listed in Table 2-1.

Table 2-1: Characteristics of the six shear walls studied

Wall	Length	Tie	Gravity	Wall	Length	Tie	Gravity
W_S	1.22 m	No	No	W_L	3.66 m	No	No
W_{ST}	1.22 m	233.5 kN/mm	No	W_{LT}	3.66 m	233.5 kN/mm	No
W_{SV}	1.22 m	No	80 kN/m	W_{LV}	3.66 m	No	80 kN/m

The material properties for the FEM of the above six shear walls were adopted from Mi (2004) and Winkel (2006), who conducted a series of experimental tests. Orthotropic material properties were selected for both the frame members and OSB sheathing panels. Table 2-2 summarizes the material properties for the frame members and OSB sheathing panels used in this study. The behaviours of SF and FF nails were also tested by Mi (2004) and Winkel (2006). The axial compressive property of FF nails was determined to be linear with a stiffness value of 106.8 kN/mm. A plot of the FF axial tensile property is shown in Figure 2-8(a). The shear property of FF nails is provided in Figure 2-8(b). SF nails are used for withstanding the shear force in this study. Figure 2-9 illustrates the shear properties of SF nails in the vertical and horizontal directions.

Table 2-2: Material properties of the frame and the OSB panel (Mi, 2004; Winkel, 2006)

Element	Density (kg/m^3)	Modulus of Elasticity (MPa)			Poisson's Ratio			Shear Modulus (MPa)		
		E_x	E_y	E_z	n_{xy}	n_{xz}	n_{yz}	G_{xy}	G_{xz}	G_{yz}
Frame	510	12,000	900	500	0.3	0.3	0.3	900	700	50
OSB	450	3,000	5,000	3,000	0.3	0.3	0.15	1,200	1,700	1,200

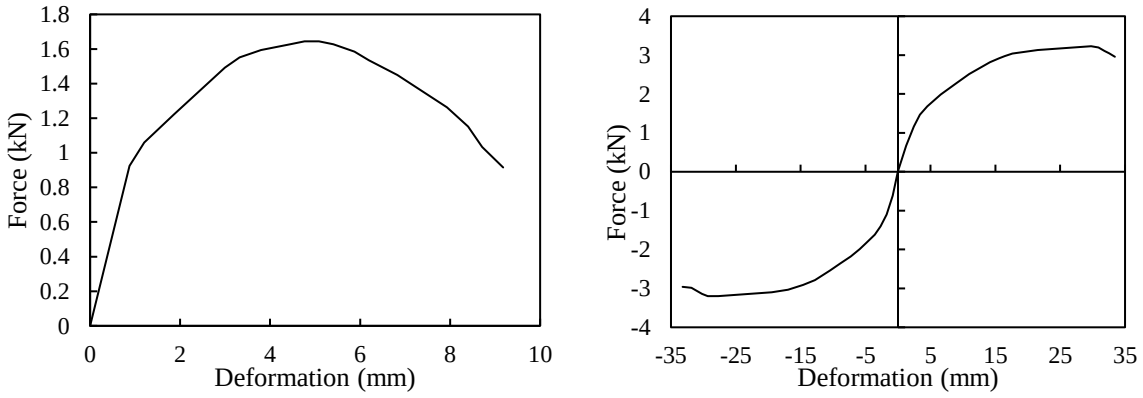

(a) Axial tensile behaviour **(b) Shear behaviour**

Figure 2-8: FF nail properties: (a) axial tensile behaviour; (b) shear behaviour (Winkel, 2006)

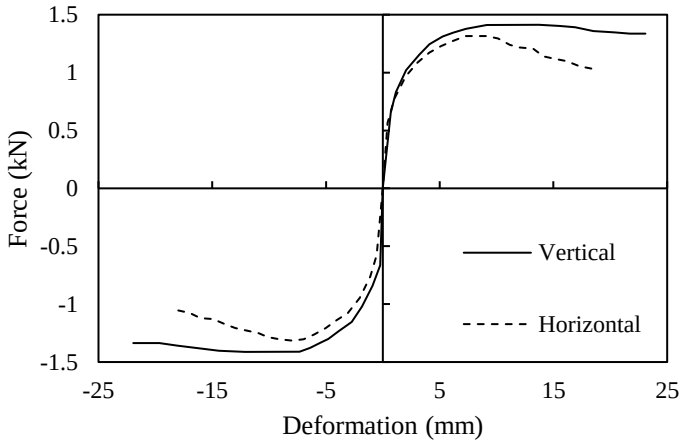

Figure 2-9: Shear properties of SF nails (Winkel, 2006)

High-resolution models for W_S, W_L, W_{ST}, W_{LT}, W_{SV}, and W_{LV} were established using the FEM method proposed by Niazi et al. (2018), as described in detail in section 2.2. In the study presented here, the base boundary condition was assumed to be a hinge support.

2.4.2 Displacement component

Using Step 2 to Step 5 from section 2.3.1, the *P-d* curve was decomposed into P-d_f and P-d_s for each of the six shear walls. Plots for these displacement components for each of the six shear walls are shown in Figure 2-10.

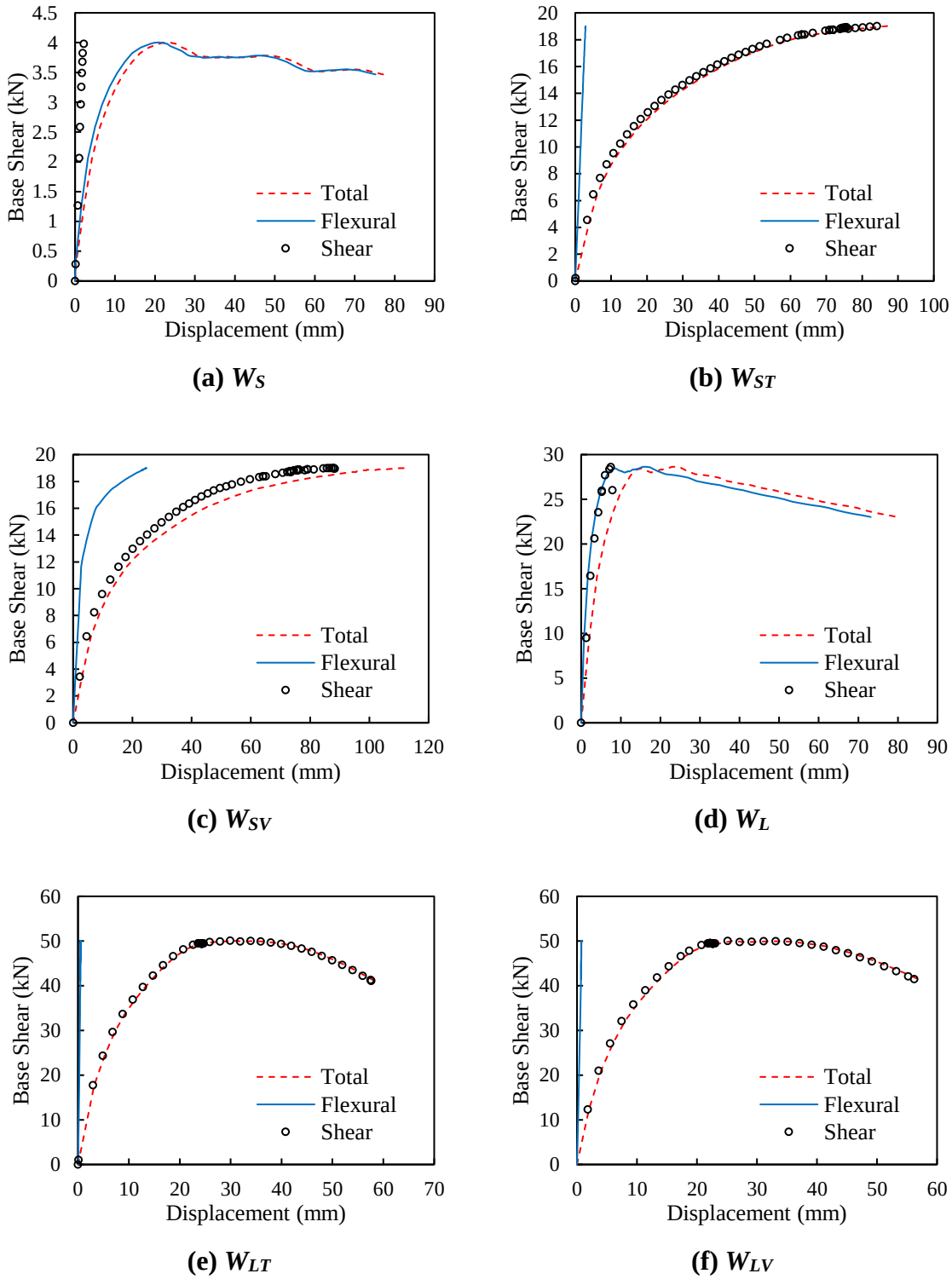

(a) W_S **(b) W_{ST}**

(c) W_{SV} **(d) W_L**

(e) W_{LT} **(f) W_{LV}**

Figure 2-10: Displacement components: (a) W_S; (b) W_{ST}; (c) W_{SV}; (d) W_L; (e) W_{LT}; (f) W_{LV}

A comparison of the displacement components of the W_S and W_{ST} walls clearly reveals that a tie rod can increase flexural stiffness and make the wall more sensitive to shear failure. The ability of the W_{ST} wall to resist the lateral load is 387% greater than that of the W_S wall, which is attributable to the fact that the W_S wall is dominated by flexural failure and does not reach its shear strength. The addition of a tie rod on two sides of the wall provides the W_{ST} wall with more flexural strength so that its shear strength can be achieved without failure from flexural displacement. Like the W_{ST} wall, the W_{SV} wall also reached its shear strength, indicating that, as with the tie rod, the gravity load can also increase flexural stiffness because it acts against the overturning of the shear wall due to the lateral load, hence increasing the flexural stiffness.

W_L is twice as long as W_S, but its peak lateral load resistance is 5.9 times greater than that of W_S, which indicates that the ability of the wall to resist the lateral load does not expand linearly with the length of the wall. A comparison of the W_L and W_S displacement components shows the same effect as with the tie rod and gravity load: increasing the length of the wall can also increase its flexural stiffness. The W_{LT} tie rod and the W_{LV} gravity load enhanced the ability to resist lateral load by 78.5% compared to W_L. This finding indicates that, for a shear wall with a small aspect ratio (height over width), tie rods and gravity loads contribute less to the ability resisting lateral load than for a wall with a large aspect ratio. For both W_{LT} and W_{LV}, the flexural displacement component is negligible compared with the shear displacement component. The P-d_s curve almost captures the global pushover analysis result P-d, which means that the total pushover analysis result P-d is dominated by P-d_s.

2.4.3 Spring characteristics

P-d_f and P-d_s curves of the six shear walls, as presented in section 2.4.2, were transformed into link tensile and shear properties in the load-displacement function of each wall's simplified model. The value of compressive stiffness can be calculated using Step 1 from section 2.3.1. The properties of the links in the axial and shear directions can be plotted as shown in Figure 2-11.

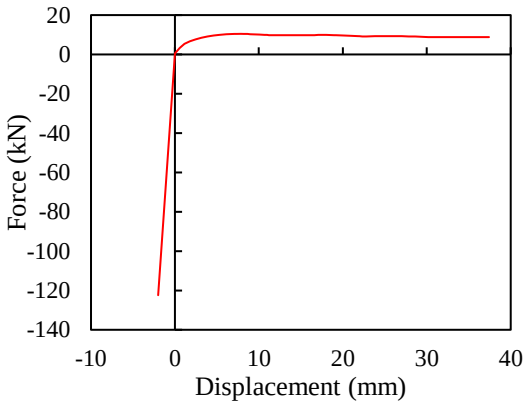

(a) W_S Axial property

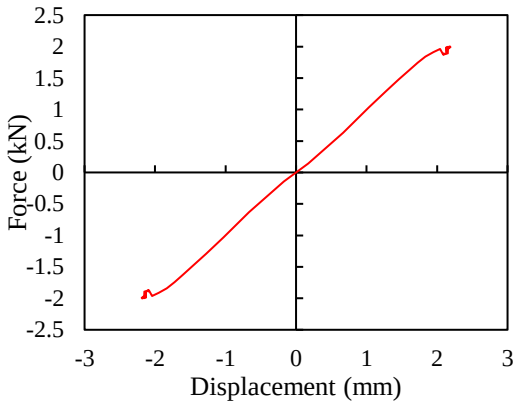

(b) W_S Shear property

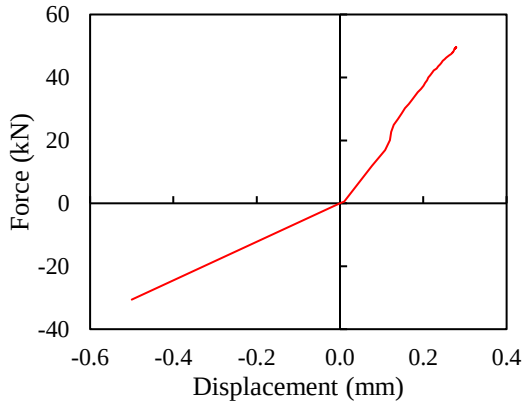

(c) W_{ST} Axial property

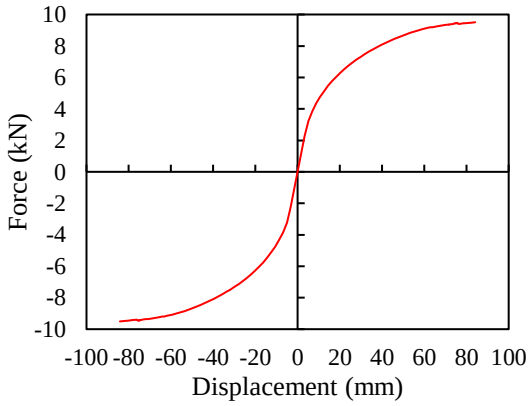

(d) W_{ST} Shear property

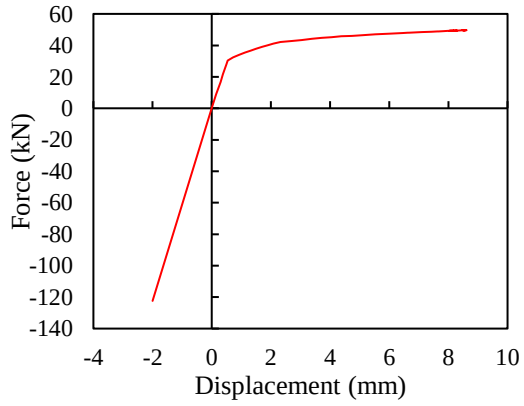

(e) W_{SV} Axial property

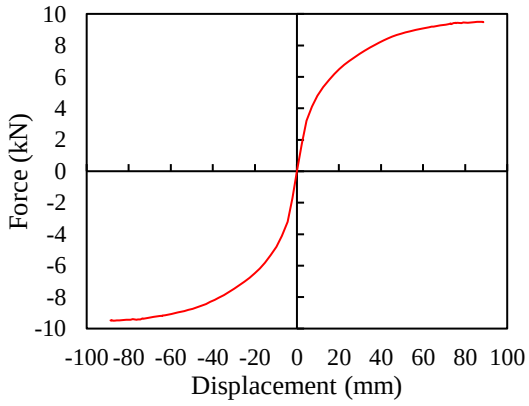

(f) W_{SV} Shear property

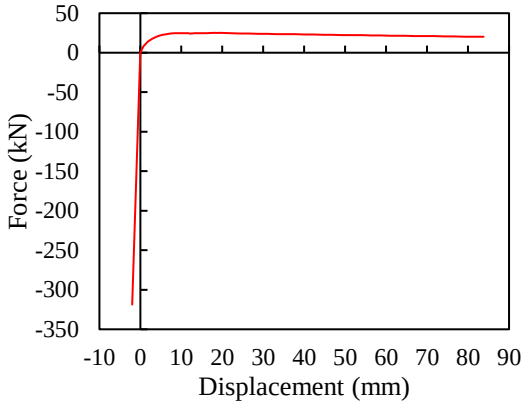

(g) W_L Axial property

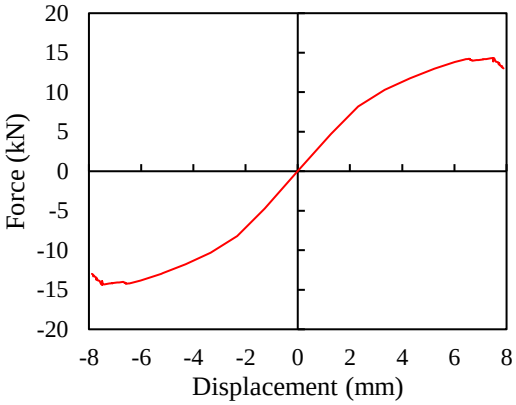

(h) W_L Shear property

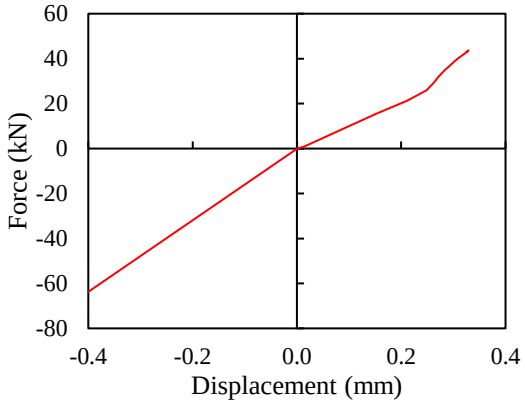

(i) W_{LT} Axial property

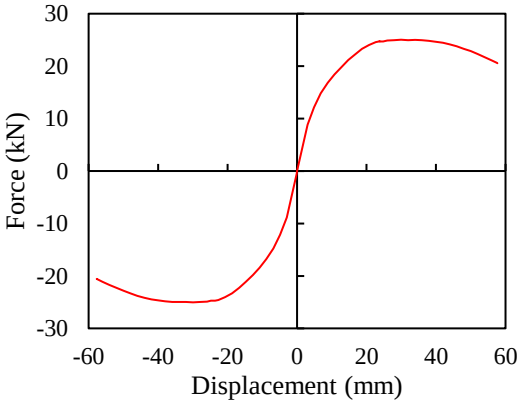

(j) W_{LT} Shear property

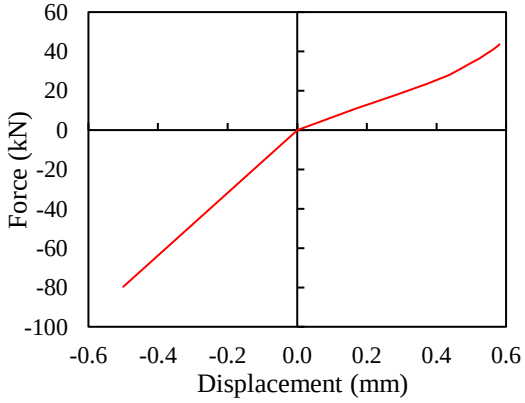

(k) W_{LV} Axial property

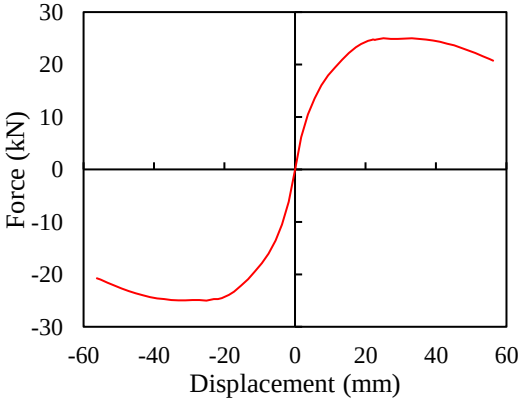

(l) W_{LV} Shear property

Figure 2-11: Spring characteristics: axial (a) and shear (b) properties of W_S; axial (c) and shear (d) properties of W_{ST}; axial (e) and shear (f) properties of W_{SV}; axial (g) and shear (h) properties of W_L; axial (i) and shear (j) properties of W_{LT}; axial (k) and shear (l) properties of W_{LV}

2.4.4 Validation of the simplified model results

The properties of the links in the axial and shear directions were applied to the simplified model of each shear wall, and the pushover analysis results were compared with the high-resolution model results, as indicated in Figure 2-12.

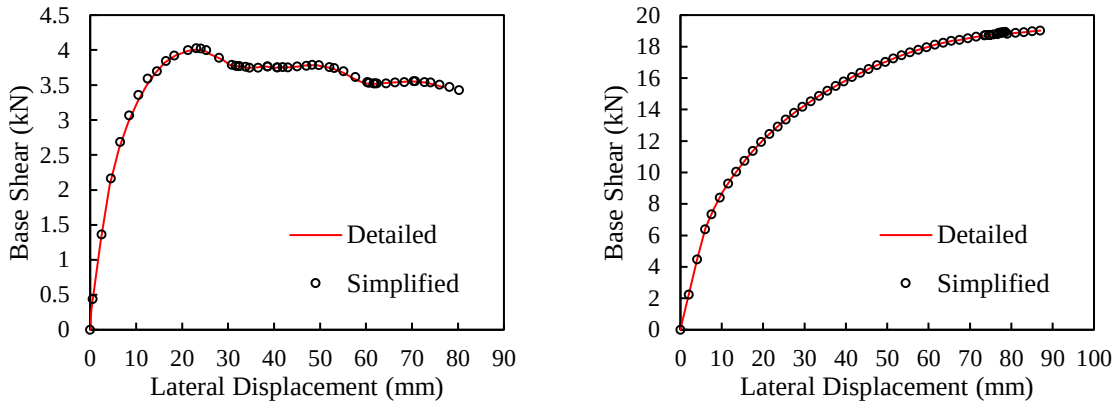

(a) W_S **(b) W_{ST}**

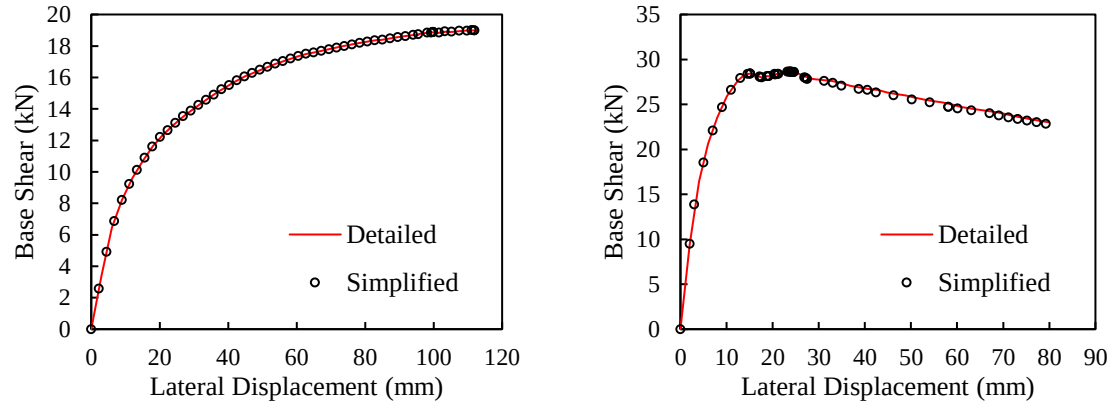

(c) W_{SV} **(d) W_L**

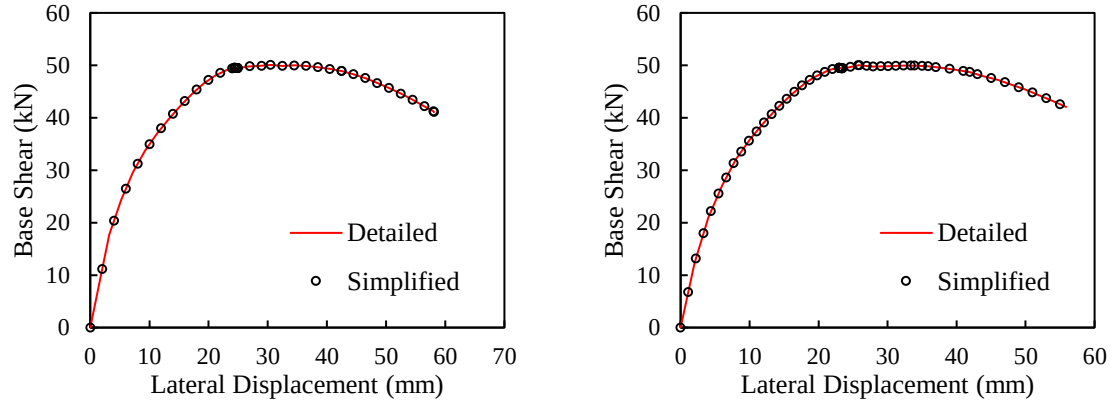

(e) W_{LT} **(f) W_{LV}**

Figure 2-12: Validation of the simplified model results for (a) W_S ; (b) W_{ST}; (c) W_{SV}; (d) W_L; (e) W_{LT}; (f) W_{LV}

For each of the six shear walls, the high-resolution and simplified FEM pushover analysis results agree very well with respect to both the ascending and descending stages. This outcome demonstrates the accuracy offered by the use of the simplified modelling procedure for a single-storey single-wall structure.

2.4.5 Single-storey single-wall simplified model database

To conduct simplified FEM, corresponding high-resolution FEM must first be established in order to obtain the properties of the simplified model links. A database consisting of commonly used high-resolution shear wall models with varied details (i.e., stud size, nail size and spacing, sheathing type, and gravity load) can be established in the future work so that the simplified model link properties for the structural details of any kind of shear wall can be easily obtained by design engineers without the necessity of completing the simplified procedure set out in section 2.3.1. This technique allows the wide use of the simplified FEM for industrial design and analysis processes.

2.5 Simplified modelling for a multi-storey single wall

2.5.1 Floor connection

The structural components of a floor system resemble those of a shear wall system, including joist framing, sheathing, and fastenings. The floor system in a real building usually connects the upper- and lower-storey shear walls with the use of bolts. However, as a research topic, high-resolution floor system modelling requires a great deal of effort and was not the focus of the study presented here. For this study, a series of very short rigid link elements connecting the bottom plate of the upper-storey shear wall and top plate of the lower-storey shear wall were adopted, but the sheathing panels were not connected (Figure 2-13). This kind of FEM is based on the assumption that the floor system is rigid with no relative deformation between the upper-storey bottom plate and the lower-storey top plate. This assumption is reasonable because, in reality, the upper-storey bottom plate and the lower-storey top plate are bolted or nailed together, resulting in a very strong degree of stiffness.

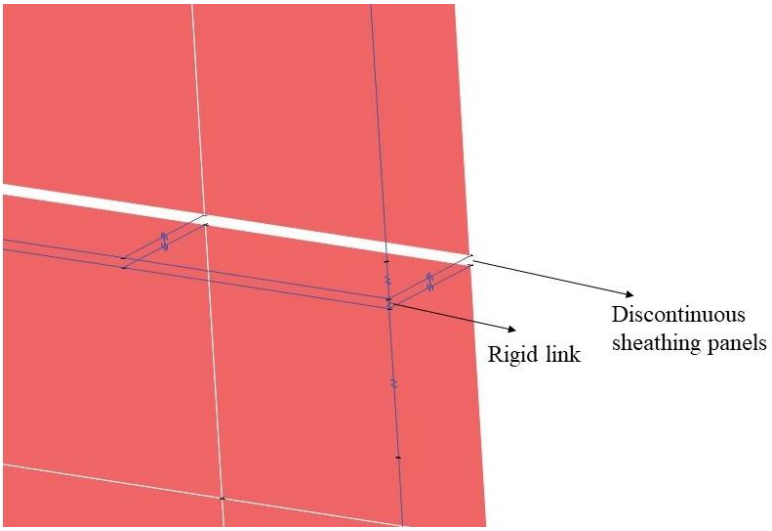

Figure 2-13: Connection between two adjacent storeys in the high-resolution FEM

2.5.2 Modelling procedure

The philosophy underlying the simplified multi-storey modelling is to make the upper-storey boundary conditions conform to those of the first storey so that the proposed single-storey simplified approach can be applied for upper storeys of the multi-storey shear walls. The rigid links (Figure 2-13) adopted for connecting the lower-storey top plate with the upper-storey bottom plate can simulate exactly the first-storey boundary condition: a rigid foundation. Figure 2-14 shows an example of a two-storey simplified model, in which the second-storey boundary condition is a pin connection, thus permitting rotation in all directions, in exactly the same way as with the first-storey hinge support. With such a modelling technique, the flexural and shear spring properties of a storey are affected only by the structural details and gravitational load of that storey. The database of single-storey simplified models to be established in the future work can be used for upper storeys, thus avoiding the necessity of establishing a multi-storey simplified model database. The gravitational load on the first storey of the structure shown in Figure 2-14 has four components: the self-weights of the first and second storeys and the floor loads acting on the first and second storeys. These gravitational loads must be considered accurately using the method illustrated in Figure 2-6 when the high-resolution model of the first storey is established.

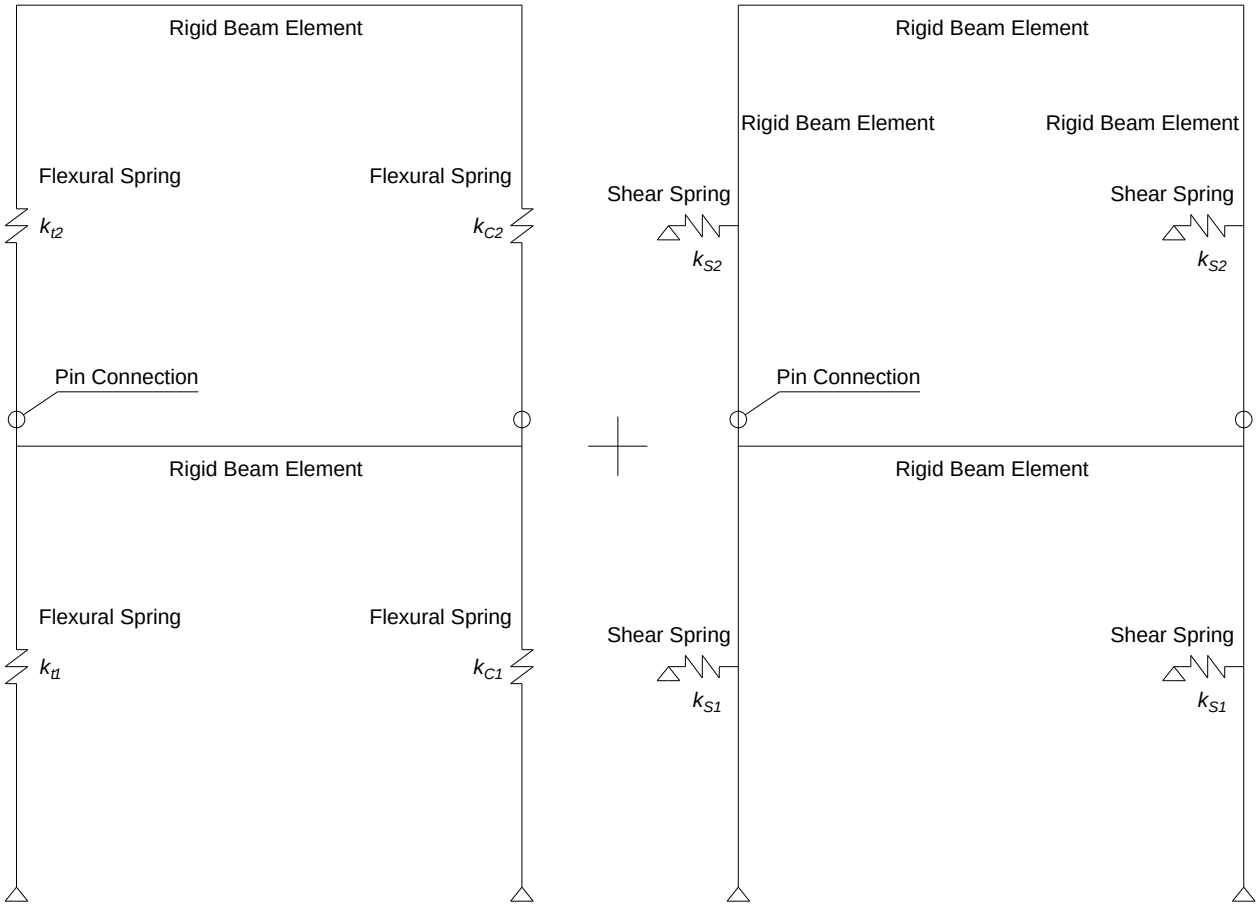

Figure 2-14: Multi-storey simplified model

2.5.3 Analysis results

W_S, W_L, W_{ST}, and W_{LT} were replicated as four-storey structures. For each four-storey structure, although each storey has the same structural details, the gravity load acting on it is different because of the accumulation of the gravity load from the other storeys. To represent these differences in the gravity loads, different high-resolution single-storey single-wall models were developed. The high-resolution model pushover analysis result for each storey was transformed into links' properties of the corresponding storey of the simplified four-storey model. Comparisons of the pushover analysis results for both the high-resolution and the simplified models of the W_S, W_L, W_{ST}, and W_{LT} types of four-storey shear walls are presented in Figures 2-15 to 2-18.

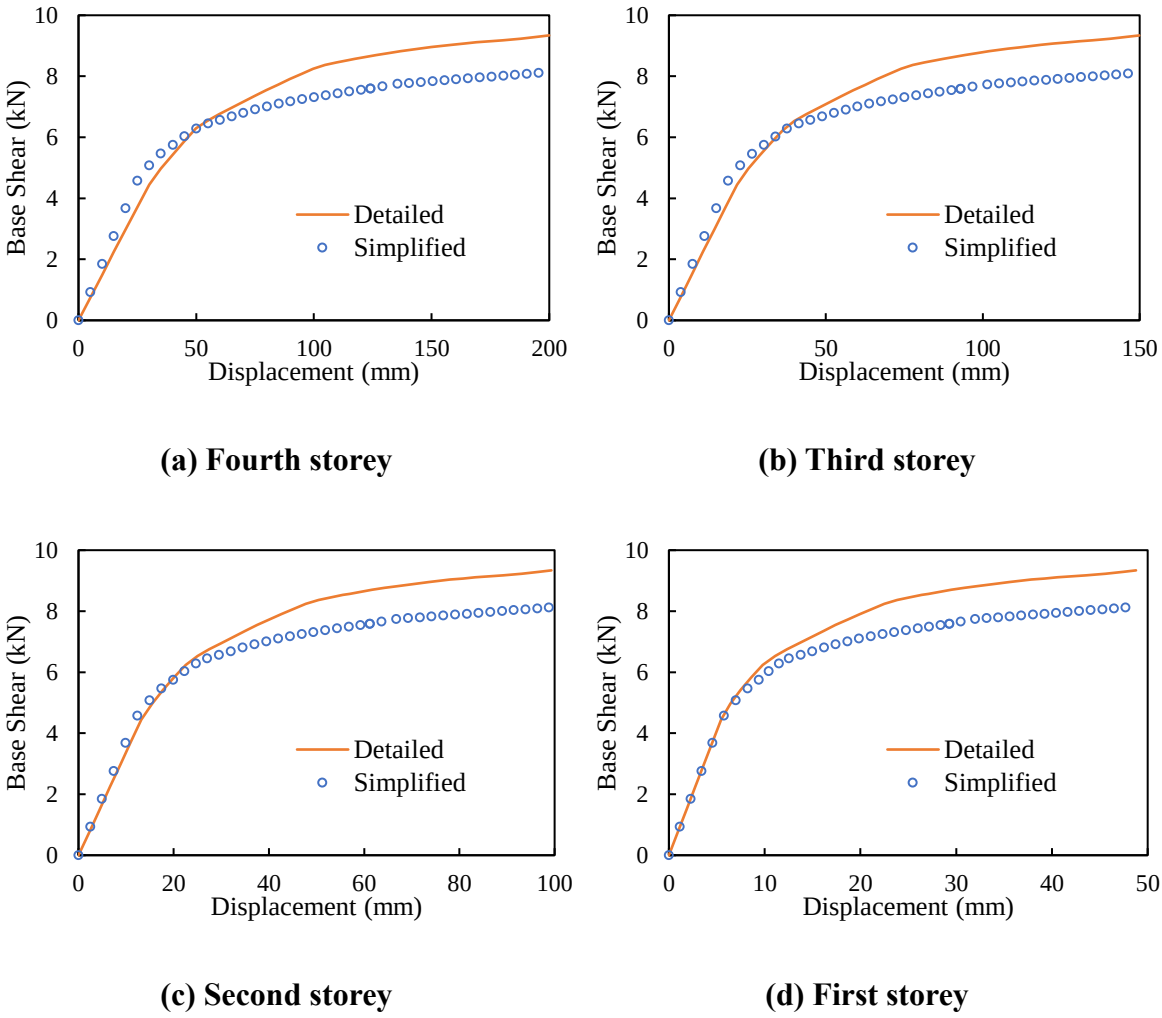

Figure 2-15: Comparison of high-resolution and simplified analysis results for the W_S type of four-storey shear wall: (a) fourth storey; (b) third storey; (c) second storey; (d) first storey

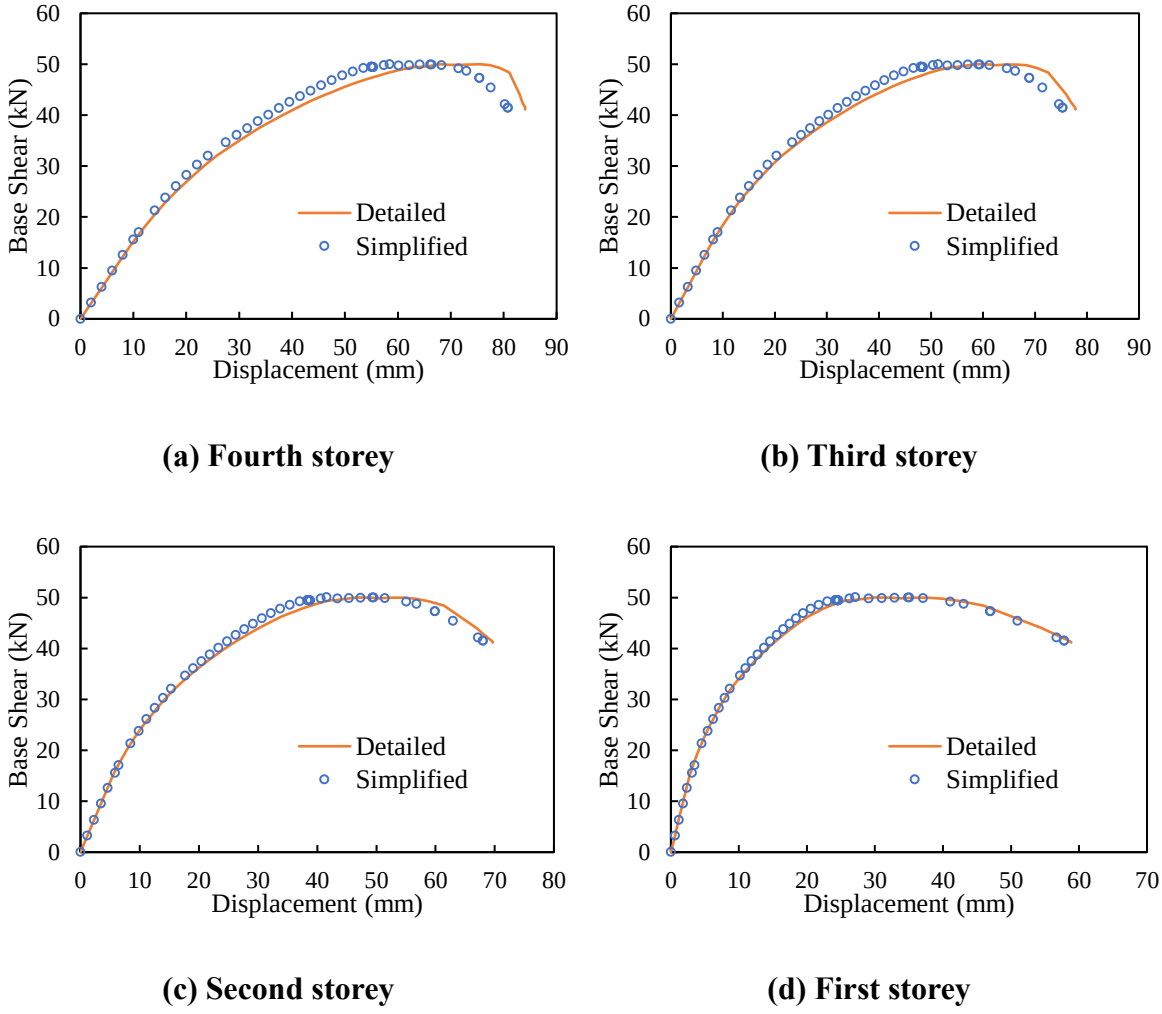

Figure 2-16: Comparison of high-resolution and simplified analysis results for the W_L type of four-storey shear wall: (a) fourth storey; (b) third storey; (c) second storey; (d) first storey

The bending effect of the frame members, which is ignored in the assumptions underlying the simplified FEM, has little influence on small-aspect-ratio shear walls because structural behaviour is dominated by shear. The W_S type of four-storey shear wall has a very large aspect ratio of 10.5, but the simplified model result is still good, with a 13.2% underestimation in strength, and a maximum of 15% overestimation in initial stiffness at the fourth storey. The difference in initial stiffness at the first storey is 1.7% overestimation because lower storeys are subject to a smaller portion of the lateral displacement caused by frame bending. With each increase in the level of the storey, the

bending effect becomes more apparent and the accumulated errors increase. High-aspect-ratio shear walls are usually strengthened with the addition of a tie rod at both ends of a shear wall, in such a way that the bending of the framing becomes less important. The simplified analysis results for the W_L type of four-storey wall are nearly identical for the ascending stage until the descending stage of the third- and fourth-storey results begin to diverge and exhibit discrepancies. The initial stiffness and the ductility values in the high-resolution and simplified FEM are in very good agreement, which indicates the ability of the simplified method to capture accurately the actual structural behaviour.

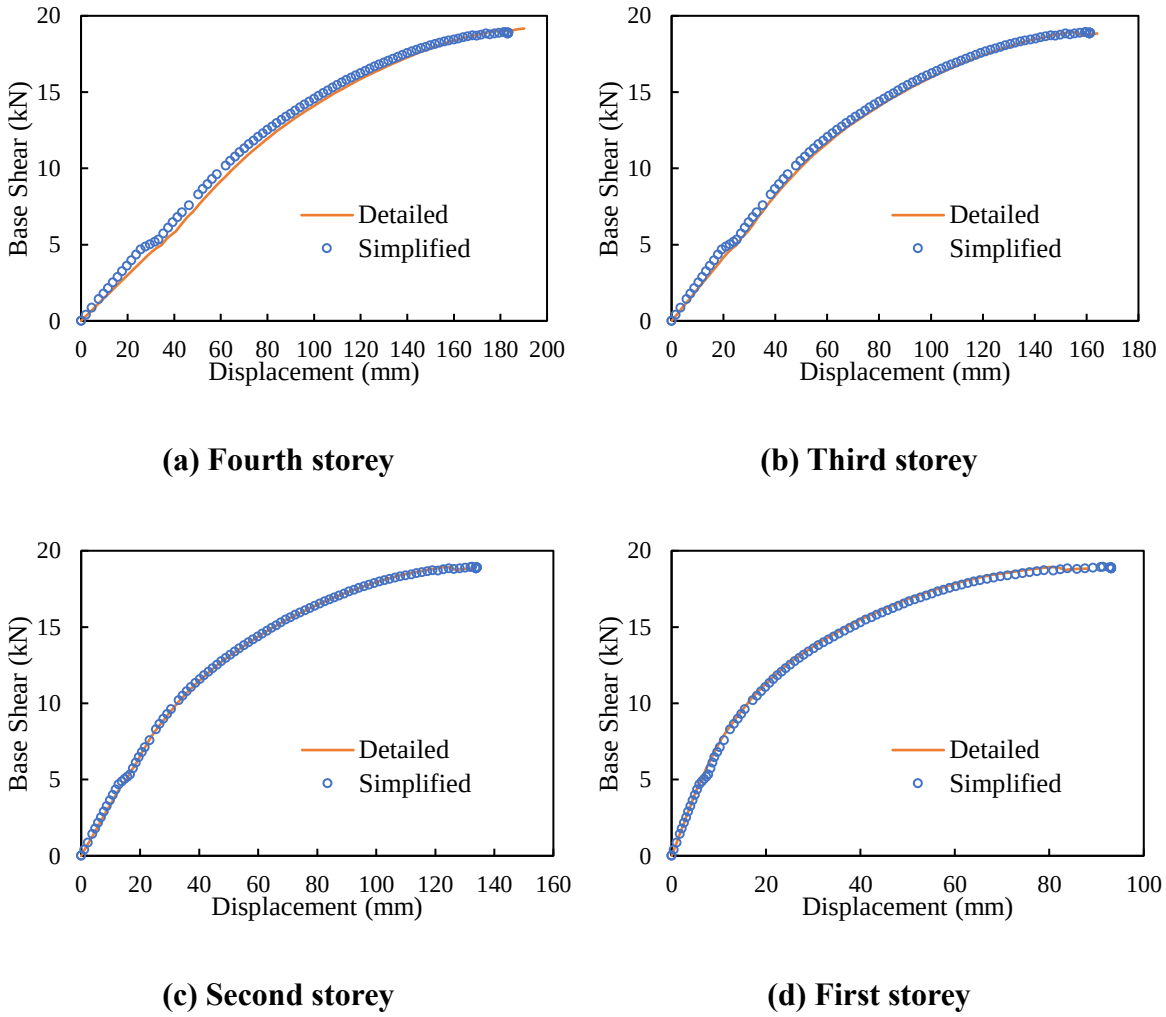

Figure 2-17: Comparison of high-resolution and simplified analysis results for W_{ST} type four-storey shear wall: (a) fourth storey; (b) third storey; (c) second storey; (d) first storey

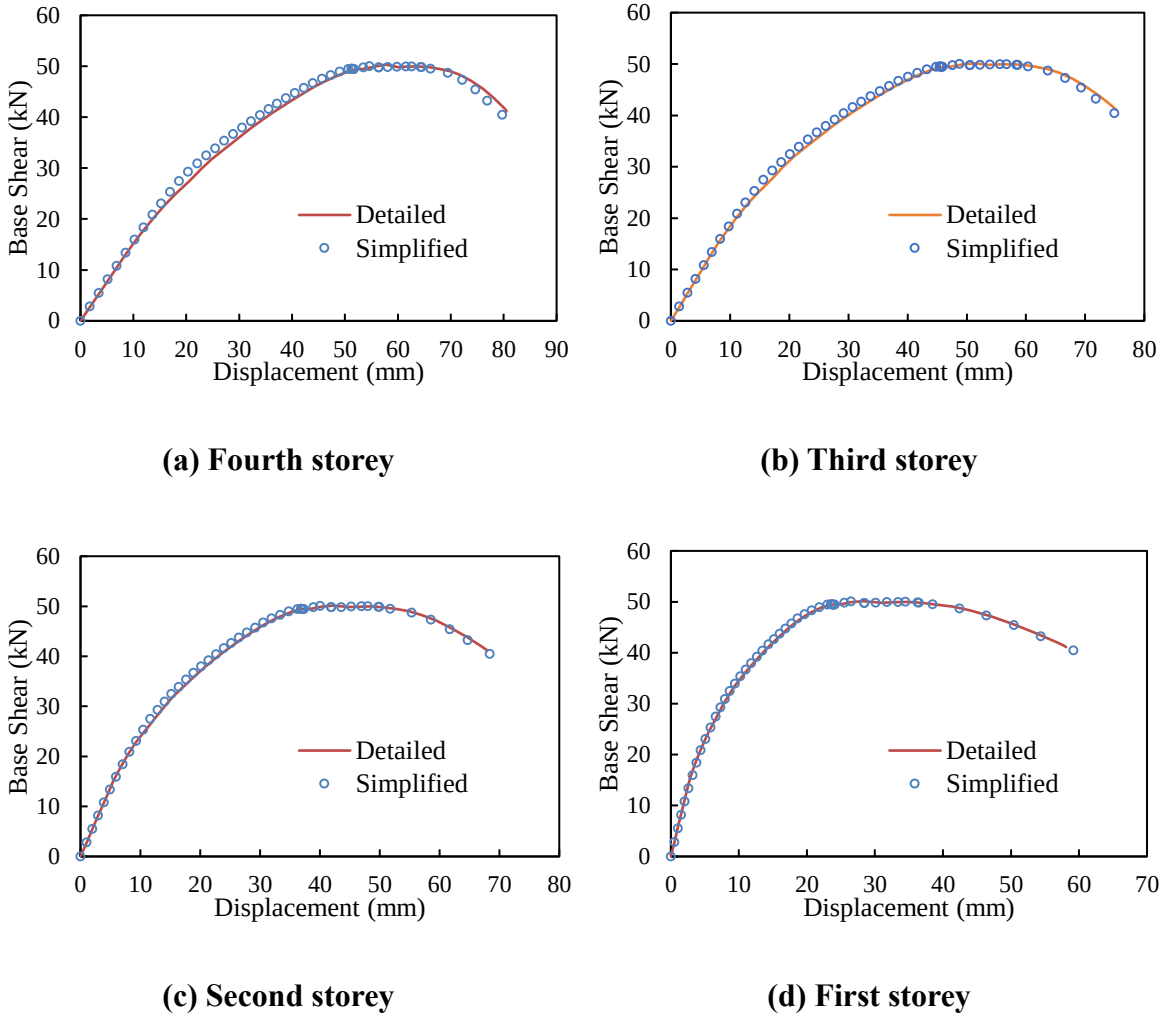

Figure 2-18: Comparison of high-resolution and simplified analysis results for W_{LT} type four-storey shear wall: (a) fourth storey; (b) third storey; (c) second storey; (d) first storey

The simplified model results compare well with those of the high-resolution models for both the W_{ST} and W_{LT} types of four-storey shear walls. The findings further validate the accuracy of the simplified procedure set out in section 2.3.1 and section 2.5.2 when it is applied to high-aspect-ratio walls with tie rods at both ends, a device widely used for high-aspect-ratio shear walls.

2.6 Summary and conclusions

A simplified FEM procedure has been developed for improving the modelling and analysis efficiency of high-resolution FEM. The simplified FEM model incorporates two side-links connected by a rigid beam element which forms the exterior skeleton. The simplified FEM procedure is derived based on an equal external and internal work approach. A high-resolution FEM pushover analysis must first be conducted so that a lateral displacement versus base shear function, and a side stud relative vertical displacement versus base shear function can be obtained. Based on the assumption that high-resolution model frame members have no bending effect, the side stud relative vertical displacement versus base shear function is transformed into a lateral flexural displacement versus base shear function. Subtracting the lateral flexural deformation from the total deformation gives the shear deformation. The equal work approach relates the tensile spring stiffness to the lateral flexural displacement versus base shear function. Nonlinear tensile spring and shear spring stiffness values can be obtained from the iteration of the simplified procedure. The clear advantages of the new procedure include efficient and accurate modelling and analysis, which makes it suitable for practical use by engineers in industry applications. The simplified method was verified for six single-storey shear walls with differing aspect ratios, tie rods, and gravity loads. Displacement component and simplified model link properties for the six shear walls were also plotted. The use of the simplified method was also verified for four multi-storey shear walls. The following conclusions can be drawn:

1. For both single-storey and multi-storey shear wall structures with varied structural details, the proposed equal-work-based simplified procedure is capable of providing good pushover analysis results with respect to lateral displacement against base shear. For all six single-storey shear walls, the pushover analysis results with both the high-resolution and the simplified FEM are almost identical. Good accuracy was also obtained for a multi-storey shear wall with a small aspect ratio (3.5), both with and without tie rods. Compared with the high-resolution model results for a high-aspect-ratio (10.5) multi-storey shear wall without tie rods, the simplified model produced 13.2% less strength and a maximum of 15%

greater initial stiffness. Strengthening this very critical high-aspect-ratio LFWS shear wall with the addition of tie rods at both ends is a widely adopted design, and the simplified method can accurately simulate almost the identical strength and stiffness of such a high-aspect-ratio multi-storey shear wall with tie rods.

2. The good agreement between the simplified and the high-resolution FEM analysis further validates the method of separating flexural and shear displacement from the total displacement. This separation method offers a valuable tool for studying LFWS displacement components and the structural response for different components.
3. Shear walls with a small aspect ratio are more dominated by shear displacement than shear walls with a high aspect ratio. Tie rods and gravity loads acting on the wall can add significant flexural stiffness to the wall, thus making it more vulnerable to shear failure. Adding tie rods and gravity loads on large-aspect-ratio shear walls can greatly increase lateral load resistance because the shear strength can be obtained without prior flexural failure. The ability of the W_{ST} and W_{SV} walls to resist lateral loads is 387% greater than that of the W_S wall. However, the tie rods in the W_{LT} and the gravity load in the W_{LV} walls increase the lateral load resistance ability by 78.5% compared to that of W_L, indicating that the addition of tie rods and gravity loads to small-aspect-ratio shear walls contributes less to the capacity to resist lateral loads.
4. The capacity of a shear wall to resist lateral loads does not increase linearly with wall length. W_L is twice as long as W_S, however, its peak lateral load resistance is 5.9 times greater than that of W_S.

In the future, a database that incorporates commonly used structural details and gravity loads can be established and can be embedded into any commercial FEM software, thus enhancing the ease with which engineers in academia and industry can build simplified shear wall FEM for their designs and analysis. The database can be established following sensitive analysis of the high-resolution shear wall model so that the database can be reduced.

2.7 References

ATS. (2008). *Strong-Rod Systems for Multi-Storey Overturning Restraint*. In *Simpson Strong-Tie*.

Baber, T. T., & Noori, M. N. (1985). Random vibration of degrading, pinching systems. *Journal of the Engineering Mechanics Division*, *111*(8), 1010–1026. https://doi.org/10.1061/(ASCE)0733-9399(1985)111:8(1010)

Baber, T. T., & Wen, Y.-K. (1981). Random Vibration Hysteretic, Degrading Systems. *Journal of the Engineering Mechanics Division*, *107*(6), 1069–1087.

Boudaud, C., Humbert, J., Baroth, J., Hameury, S., & Daudeville, L. (2015). Joints and wood shear walls modelling II: Experimental tests and FE models under seismic loading. *Engineering Structures*, *101*, 743–749. https://doi.org/10.1016/j.engstruct.2014.10.053

Casagrande, D., Rossi, S., Sartori, T., & Tomasi, R. (2016). Proposal of an analytical procedure and a simplified numerical model for elastic response of single-storey timber shear-walls. *Construction and Building Materials*, *102*, 1101–1112. https://doi.org/10.1016/j.conbuildmat.2014.12.114

Chen, Z., Chui, Y. H., Ni, C., Mohammad, M., & Doudak, G. (2014). Simulation of the lateral drift of multi-storey light wood frame buildings based on a modified macro-element model. *WCTE 2014 - World Conference on Timber Engineering*, 1–9. Quebec City, Canada.

Collins, M., Kasal, B., Paevere, P., & Foliente, G. C. (2005). Three-Dimensional Model of Light Frame Wood Buildings. I: Model Description. *Journal of Structural Engineering*, *131*(4), 676–683. https://doi.org/10.1061/(ASCE)0733-9445(2005)131

CSA-O86. (2014). Engineering Design in Wood. In *Canadian Standards Association*. Retrieved from http://shop.csa.ca/en/canada/structures/o86-09-consolidation/invt/27013742009

CSI. (2016). Analysis Reference Manual for SAP2000, ETABS, SAFE and CSiBridge. In *Computers and Structures, Inc.* Retrieved from http://docs.csiamerica.com/manuals/etabs/Analysis Reference.pdf

Filiatrault, A., Isoda, H., & Folz, B. (2003). Hysteretic damping of wood framed buildings. *Engineering Structures*, *25*(4), 461–471. https://doi.org/10.1016/S0141-0296(02)00187-6

Folz, B., & Filiatrault, A. (2000). CASHEW - Version 1.0: A computer program for cyclic analysis of wood shear walls. In *Management*.

Foschi, R. O. (2000). Modeling the hysteretic response of mechanical connections for wood structures. *6th World Conference on Timber Engineering*, 1–11. Whistler, Canada.

Gu, J. Z., & Lam, F. (2004). Simplified mechanics-based wood frame shear wall model. *13th World Conference on Earthquake Engineering*, 1–11. Vancouver, B.C., Canada.

Humbert, J., Boudaud, C., Baroth, J., Hameury, S., & Daudeville, L. (2014). Joints and wood shear walls modelling I: Constitutive law, experimental tests and FE model under quasi-static loading. *Engineering Structures*, *65*, 52–61. https://doi.org/10.1016/j.engstruct.2014.01.047

Itani, R. Y., & Cheung, C. K. (1984). Nonlinear analysis of sheathed wood diaphragms. *Journal of Structural Engineering*, *110*(9), 2137–2147.

Kuzman, M. K., & Sandberg, D. (2017). Development of Multi-Storey Timber Buildings and Future Trends. *II Latin American Congress on Timber Structures*, 1–7. Junin, Argentina.

Li, M., Lam, F., Foschi, R. O., Nakajima, S., & Nakagawa, T. (2012). Seismic performance of post and beam timber buildings I: Model development and verification. *Journal of Wood Science*, *58*(1), 20–30. https://doi.org/10.1007/s10086-011-1219-5

Mi, H. (2004). *Behavior of unblocked wood shear walls* (University of New Brunswick, Fredericton, Canada).

NBCC. (2015). *National Building Code of Canada*. National Research Council of Canada, Ottawa, Canada.

Niazi, M., El Damatty, A., & Hamada, A. (2018). Sensitivity study of the light-framed wood shear walls subjected to lateral loads. *6th International Structural Specialty Conference 2018, Held as Part of the Canadian Society for Civil Engineering Annual Conference 2018*, 1–9. Fredericton, Canada.

Pfretzschner, K. S., Gupta, R., & Miller, T. H. (2014). Practical modeling for wind load paths in a realistic light-frame wood house. *Journal of Performance of Constructed Facilities*, *28*(3), 430–439. https://doi.org/10.1061/(ASCE)CF.1943-5509.0000448

Rossi, S., Casagrande, D., Tomasi, R., & Piazza, M. (2016). Seismic elastic analysis of light timber-frame multi-storey buildings: Proposal of an iterative approach. *Construction and Building Materials*, *102*, 1154–1167. https://doi.org/10.1016/j.conbuildmat.2015.09.037

Stewart, W. G. (1987). *The seismic design of plywood sheathed shear walls*. University of Canterbury, Christchurch, New Zealand.

Winkel, M. H. (2006). Behavior of light-frame walls subject to combined in-plane and out of plane loads (University of New Brunswick, Fredericton, Canada). Retrieved from http://scholar.google.com/scholar?hl=en&btnG=Search&q=intitle:Behavior+of+light-frame+walls+subject+to+combined+in-plane+and+out+of+plane+loads#0

Winkel, M., & Smith, I. (2010). Structural behavior of wood light-frame wall segments subjected to in-plane and out-of-plane forces. *Journal of Structural Engineering*, *136*(7), 826–836. https://doi.org/10.1061/(ASCE)ST.1943-541X.0000170

Xu, J., & Dolan, J. D. (2009a). Development of a wood-frame shear wall model in ABAQUS. *Journal of Structural Engineering*, *135*(8), 977–984. https://doi.org/10.1061/(ASCE)ST.1943-541X.0000031

Xu, J., & Dolan, J. D. (2009b). Development of nailed wood joint element in ABAQUS. *Journal of Structural Engineering*, *135*(8), 968–976. https://doi.org/10.1061/(ASCE)ST.1943-541X.0000030

Chapter 3

3 High-Resolution and Simplified Numerical Modelling of a Four-Storey Light-Frame Wood Building

3.1 Introduction

The National Building Code of Canada NBCC (2015) currently allows up to 6 stories of light-frame wood structure (LFWS) buildings. However, current design method for LFWS buildings is still based on hand calculation, which yields either unsafe or too conservative results. This deficiency results from the complex structural details of LFWS, which make the numerical modelling and analysis too time-consuming. Nowadays, the rapid development of computer technology enables researchers to conduct high-resolution FEM of 3D LFWS buildings with all structural details (i.e., frame members, sheathing panels, and their fasteners) considered.

A few of previous studies were conducted for the high-resolution FEM of 3D LFWS buildings to study the static, dynamic, and load sharing behaviour of the buildings. These studies featured a remarkable step forward the better understanding of the behaviour of LFWS buildings at 3D level. Collins et al. (2005a) proposed a 3D full house nonlinear FEM procedure for a one-storey light-frame residential building. The building was first modelled by simplifying each shear wall as a combination of beam elements, shell elements, and two energetically equivalent diagonal nonlinear springs. Then a high-resolution FEM procedure was proposed to study the actual response of each shear wall by applying the load calculated from the 3D full house model. This more high-resolution model simulated both the sheathing panels and frame members as shell elements. The sheathing panels were connected to frame members by nails, which were modelled as zero length springs. The companion paper (Collins et al., 2005b) verified the accuracy of this proposed 3D full house nonlinear FEM. Satheeskumar et al. (2017) proposed a 3D FEM procedure of an entire house using ABAQUS (Smith, 2009) with shear walls and diaphragms to study the load sharing under wind loads. The frame members and sheathing panels of the shear walls were modelled as isotropic brick element and isotropic shell elements, respectively. Each connection between the sheathing panels and

the frame members was represented by three nonlinear spring elements with the properties obtained from individual connection test. Frame-to-frame connections were assumed as surface-to-surface tie constraints. Results obtained from this proposed FEM showed good agreement with the full-scale test conducted by Satheeskumar et al. (2016).

Due to the large amounts of nails in a LFWS building, the high-resolution FEM procedures for multi-storey LFWS buildings consume extensive time for both the modelling and analysis, particularly for dynamic analysis. This inefficiency hinders the application of the high-resolution modelling method in both academia and industry. The increasing demand for LFWS addresses the importance of finding a more effective way to model and analyze the multi-storey LFWS buildings to allow for the study of their behaviours subjected to different kinds of load. A lot of researches have further substituted the high-resolution FEM procedures by simplified FEM procedures capable of resulting in similar structural performance in terms of lateral load versus lateral displacement.

Tarabia and Itani (1997) proposed a simplified building model which consists of diaphragms and inter-component connection elements only. One diaphragm was used to represent all components of a shear wall. Shear wall diaphragms were connected to the floor diaphragm by inter-component connections. Filiatrault et al. (2003) proposed a Pancake Model to simulate the seismic response of a two-storey LFWS building. Floor diaphragms were modelled as rigid plane stress quadrilateral elements, and they were surrounded by frame elements with high axial stiffness and very small bending stiffness along the four edges of the floor diaphragms. Floor diaphragms were connected by zero-length nonlinear shear spring elements which simulated the shear walls. The properties of the nonlinear shear spring elements were obtained from the Wayne Stewart hysteresis rule (Stewart, 1987). Xu and Dolan (2009) simplified a single shear wall with a pair of diagonal springs connecting the top and bottom plates. The hysteretic properties of this spring were established upon the estimation of 13 parameters which were modified from BWBN (Baber and Noori, 1985; Baber and Wen, 1981) single nail model. Eight simplified shear walls were connected by floor diaphragms to form a 3D two-storey house which was tested by (Fischer et al., 2001). The diaphragms were modelled with

4×6 shell elements with in-plane stiffness calibrated from quasi-static test. The fundamental period and seismic time-history analysis result compared well with the experiment (Fischer et al., 2001). Pei and van de Lindt (2011) employed the shear-bending model developed by Pei and van de Lindt (2009) to model a six-storey LFWS building. Floor diaphragms were modelled using rigid plate elements. Adjacent floor diaphragms were connected by shear walls which were captured by nonlinear springs with the hysteresis estimated from the hysteretic model developed by Folz and Filiatrault (2001). Li et al. (2012) proposed a simplified numerical model called PB3D, which simulated floor and roof diaphragms as combined beam and diagonal truss elements. The truss elements were used to simulate the in-plane stiffness of the diaphragms, which were determined based on individual diaphragm test. Shear walls were calibrated by vertical beam elements and diagonal spring elements, with the spring elements' properties revised from the HYST model (Foschi, 2000). Martin et al. (2011) simplified the high-resolution FEM by eliminating the modelling of individual fasteners, and the effect of fasteners were incorporated into sheathing panels by adjusting the shear modulus of the panels. Sheathing panels were modelled as a continuous orthotropic thick-shell element with generated auto-meshing, and frame members were modelled as isotropic frame elements. Hafeez et al. (2019) established a linear 3D simplified model with each shear wall simulated by rigid frame skeletons and a horizontal spring. The properties of the spring was obtained from the first three components of the single-storey shear wall displacement equation in Canadian timber design standard CSA-O86 (2014), which takes into consideration of the wall bending, panel shear, and nail slip. respectively. This simplified 3D linear model was found capable of capturing the natural period.

Based on the study of lateral displacement sources of LFWS buildings, some analytical simplified models capable of predicting responses of multi-storey LFWS buildings were also proposed. Tomasi et al. (2015) analyzed a three-storey LFWS building by adopting the analytical approach proposed by Casagrande et al. (2012), who equated the wall stiffness to four components of the lateral displacement (i.e., sheathing panel shear deformation, shear deformation of nails on the sheathing panels, rigid body translation, and rigid body rotation) and used different springs to capture these components. Tomasi

et al. (2015) assigned each diaphragm with a horizontal constraint. Floor mass was applied in the center of the corresponding diaphragm.

Previous simplified methods either require extensive efforts in the determination of hysteresis parameters of the spring fasteners and the diaphragms or require establishment of the displacement-component-based linear analytical models. Simplified multi-storey LFWS building models that can be efficiently used by design engineers with good degree of accuracy are still in great need. This demand leads to the purpose of the study in this chapter, which is to further extend the developed simplified FEM method mentioned in Section 2.3 for single-storey wall and Section 2.5 for multi-storey wall to complex 3D LFWS buildings.

This chapter is structured as follows: A high-resolution FEM method for multi-storey 3D LFWS buildings is first presented. A case study is then carried out by applying this FEM method to an actual building, which has been recently completed in Ontario, Canada. The frequencies of this high-resolution model obtained from modal analysis are compared with results from field measurements to verify the accuracy of this high-resolution FEM method. The accuracy of the extended simplified modelling procedure for 3D buildings is then validated by conducing pushover analysis using both the high-resolution and the simplified models of the actual building. In the end, the validated high-resolution FEM model is used to understand the behaviour of this LFWS building including the level of nonlinearity in the nails and the demand-to-capacity ratios of the sheathing panels and the frame members at the design loads.

3.2 Description of the structural system of an actual LFWS building

A five-storey composite residential building in Ontario, Canada was studied. The first storey requires large space and significant storey height, so reinforced concrete structural system was chosen to avoid the soft-storey effect. Four LFWS storeys are connected to the reinforced concrete storey through 175 mm long expansion anchors spaced 1220 mm apart with a diameter of 13 mm. The reinforced concrete storey can be treated as rigid ground because it is much stiffer than the LFWS storeys. This building is separated by an

expansion joint located to the east of the elevator in the middle. This expansion joint separates the building into two independent structures in terms of movement. The eastern half of the four-storey LFWS was considered in this study. The external façade of the building has some curvature to accommodate for the surrounding roads and make the best use of available land. The L-shaped four-storey LFWS, shown in Figure 3-1, has a height of 12.87 m. The long side of the L-shape has a dimension of 46.8 m long and 22.7 m wide, and the short side of the L-shape has a dimension of 16.5 m long and 9.5 m wide. Approximate area of each floor is 1219 m^2.

Figure 3-1: Composite wood-on-concrete building

The lateral load resisting system is formed by LFWS shear walls. The frame members of the shear walls are sheathed with 11.1 mm Type 1 OSB at one side by common wire nails or power-driven nails with a minimum penetration depth of 64 mm. The building load bearing walls are sheathed with 15.9 mm Type X GWB panels, which is the only allowed GWB product in the Canadian timber design standard CSA-O86 (2014). All wood posts, studs and plates of the shear walls are made of Spruce-Pine-Fir (SPF) material, and they have the same type of dimension lumber with Grade No. 1/No.2. All of the top plates and most of the end post comprise two-layered dimension lumbers. Table 3-1 shows the end posts lumber size and panel edges nail spacing of different shear walls at different storeys. The nail spacings at the interior of the panels are always 300 mm. There are two options of sizes to choose from for each end post. The selection of the size is based on consistency with stud schedule. Six types of the stud schedules are shown in Table 3-2.

Table 3-1: Schedules of end posts and nail spacing

Storey	Schedule	Type 1	Type 2	Type 3	Type 4
4	Nail Spacing (mm)	150	150	150	150
	End Posts	1-38×89 or 1-38×140	2-38×89 or 1-38×140	2-38×89 or 1-38×140	1-38×89 or 1-38×140
3	Nail Spacing (mm)	150	150	150	150
	End Posts	1-38×89 or 1-38×140	2-38×89 or 1-38×140	2-38×89 or 1-38×140	1-38×89 or 1-38×140
2	Nail Spacing (mm)	75	150	150	100
	End Posts	3-38×89 or 1-38×140	2-38×89 or 1-38×140	2-38×89 or 1-38×140	2-38×89 or 1-38×140
1	Nail Spacing (mm)	50	150	100	75
	End Posts	4-38×89 or 1-38×140	2-38×89 or 1-38×140	2-38×89 or 1-38×140	3-38×89 or 1-38×140

Table 3-2: Schedule of the stud

Type	Schedule	Type	Schedule
1	38×89mm @ 406mm	4	38×140mm @ 305mm
2	38×89mm @ 305mm	5	2-38×89mm @ 406mm
3	38×140mm @ 406mm	6	2-38×89mm @ 305mm

Figure 3-2 shows the floor plan of the LFWS storey. The interior walls are shear walls, and they are embraced externally by walls that are sheathed by GWB, which are marked in yellow. The external walls have the same stud schedule of Type 3, and the wall posts have the same size as the stud. The frame members are sheathed by 15.9 mm Type X GWB by nails spaced 150 mm apart at the exterior of the GWB and 300 mm apart at the interior of the GWB. There are thirty-one interior shear walls at each storey. Table 3-3 shows all shear wall details at every storey, in the form of “post and nail type – stud type”.

Figure 3-2: Floor plans

Note: External yellow walls are load bearing walls which are sheathed with GWB

Table 3-3: Details of all of the shear walls.

W1; W2; W3; W4; W5; W6; W22; W23	W7	W8	W9	W10
2-3; 2-3; 2-3; 2-3	2-4; 2-3; 2-3; 2-3	2-6; 2-5; 2-1; 2-1	1-2; 1-5; 1-1; 1-1	1-4; 1-4; 1-3; 1-3
W11	W12	W13; W20	W14	W15
3-3; 3-3; 3-3; 3-3	4-1; 4-1; 4-1; 4-1	3-2; 3-1; 3-1; 3-1	2-6; 2-5; 2-1; 2-1	3-2; 3-1; 3-1; 3-1
W16	W17	W18; W24; W28; W29	W19	W21
2-6; 2-5; 2-1; 2-1	4-3; 4-3; 4-3; 4-3	2-1; 2-1; 2-1; 2-1	3-6; 2-5; 2-1; 2-1	4-5; 4-2; 4-1; 4-1
W25; W26; W27; W30	W31			
4-3; 4-3; 4-3; 4-3	1-5			

Note: Shear wall details shown in the form of “post and nail type – stud type”. The four items separated by “;” represent first to fourth storey, respectively.

Floor and roof gravity loads are shown in Table 3-4. The self-weight of a floor accounts for floor joists, sheathing, and concrete topping. The design wind load acting on each floor was calculated using NBCC (2015) clause 4.1.7.3 with a reference velocity pressure

of 0.47 kPa by assuming a rectangular floor plan with dimension of 59.6 m long and 35.3 m wide. The design wind loads for the first to fourth storeys are 59 kN, 59 kN, 60 kN, and 31 kN, respectively.

Table 3-4: Gravity load details (Unit: kPa)

Floor	Self-weight	Additional dead load	Live load
1~3	1.18	0.24	5
4	0.72	0.24	1.12 (snow)

Each of the two sides of a shear wall includes a Simpson Strong-Tie tie rod (ATS, 2008) to resist the tension force resulting from lateral load. Two main structural components of the tie rod are steel rod and take-up device. Each steel rod segment is as high as the storey height, and the steel rod segments are connected by take-up devices located at the upper surface of the floors.

3.3 Description of the high-resolution FEM

The single-wall numerical FEM procedure proposed by Niazi et al. (2018) was adopted for this research to establish a 3D high-resolution model of the LFWS structural systems of the project mentioned in Section 3.2. The high-resolution 3D model was established by ETABS (CSI, 2016). The FEM procedure took into consideration all of the shear wall components including studs, top plates, bottom plates, blocking, sheathing panels, SF nails, and FF nails. Beam elements and shell elements were employed to represent the frame members and sheathing panels, respectively. Two-node link elements were used to simulate the SF and FF nails. The beam elements and shell elements were meshed manually based on the spacing of the SF nails located at sheathing panel edges. The high-resolution FEM assumed the base supports of the building were hinged at the location of the studs. The high-resolution model shown in Figure 3-3 comprises 86,411 beam elements, 216,398 shell elements and 95,743 link elements.

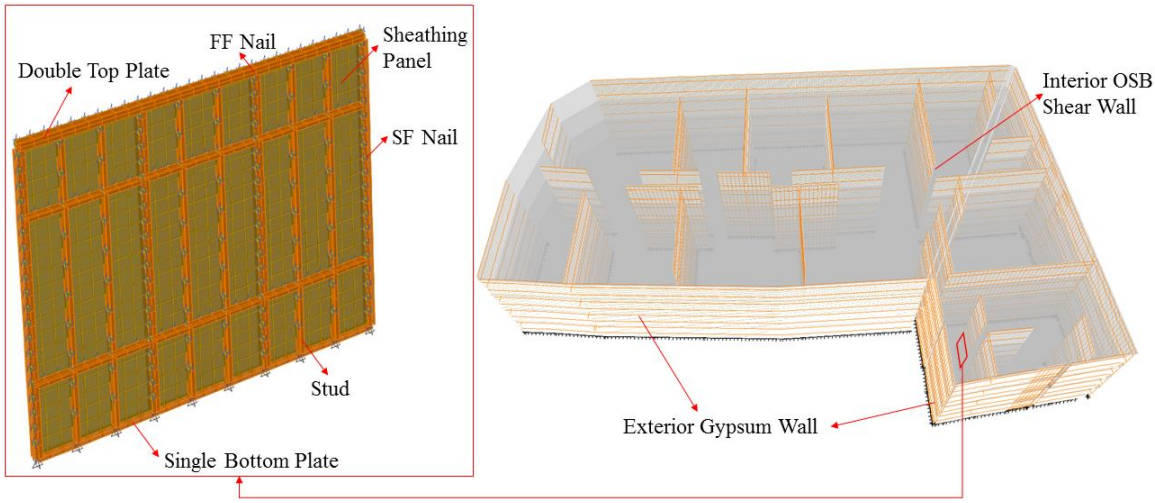

Figure 3-3: High-resolution building model

3.3.1 Material properties

The material properties for the frame members and the OSB sheathing panels used in the high-resolution FEM of the 3D building were the same as those summarized in Table 2-2.

Researchers usually do not account for the walls sheathed with GWB in high-resolution FEM. But GWB can contribute to the ability of resisting lateral load. Younquist (2000) stated that GWB has slightly higher stiffness than OSB. CSA-O86 (2014) accounted for the contribution of GWB in resisting lateral loads on condition that the interstorey drift ratio caused by seismic loading does not exceed 1% and GWB is subjected to short-term duration loading only. Such provision is probably for the consideration that GWB is brittle. This study includes a comparison of the natural frequencies obtained from high-resolution model modal analysis and a field measurement. The building had limited lateral displacement during the field measurement, indicating GWB can contribute to the lateral load sharing. For this reason, the high-resolution FEM considered the contribution of GWB in the modal analysis. But for the other studies (i.e., the simplified 3D FEM method validation and the structural performance under design loads), external walls that are sheathed with GWB were not considered. This study adopted the same isotropic material properties for GWB as Satheeskumar et al. (2017), with density of 720 kg/m^3, modulus of elasticity of 2000 MPa, and Poisson's ratio of 0.2.

3.3.2 Nail modelling

The high-resolution FEM includes the modelling of all of the FF and SF nails. The nails were modelled using two-node multi-linear elastic link elements in ETABS (CSI, 2016). The FF nails have three DOFs (i.e. axial deformation and shear deformation in two perpendicular directions), while the SF nails only have two perpendicular DOFs in shear directions. The nonlinear load-displacement relationships obtained from Mi (2004) and Winkel (2006) were assigned for these DOFs. The load-displacement relationship of each DOF was plotted in black curve in Figure 3-12.

3.3.3 Tie rod modelling

Simpson Strong-Tie tie rod (ATS, 2008) was modelled as hook element in ETABS (CSI, 2016) with only axial-elongation capacity. Cumulative lateral forces at lower storeys are larger than the lateral forces at upper storeys, thus the tension forces in the tie rods which result from lateral loads decrease with the increase of storeys. Tie rods with different stiffness were employed at different storeys to represent the differences of the tension forces. One steel rod segment of a tie rod system is connected by two take-up devices located above the adjacent slabs. The equivalent stiffness of the tie rods resulting from take-up device seating increment and steel rod elongation were determined as per Simpson Strong-Tie user manual (ATS, 2008).

3.3.4 Shell element modelling

The shear wall sheathing panels were modelled using rectangular 3D shell elements, so the system effect was simulated automatically. The sheathing panels of a shear wall were treated as continuous without considering the gaps between two adjacent dimension panels, and this modelling method assumes that the internal forces are continuously transferred in the sheathing panels. A sheathing panel comprises many continuous shell elements, with the size of each element equals to the spacing of the SF nails at the edge of the sheathing panel.

The floor and roof structural components resemble a shear wall system, which include joist framing, sheathing, and fastenings. High-resolution floor system modelling itself is a

complex research topic, thus not considered in current research which focuses on behaviour of shear walls. Floors and roof were modelled using thick-shell elements assigned with an assumed rigid diaphragm. Heights of the floors and roof were calculated by equating the actual self-weight of the structural components to the self-weight of the floors and roof in the model. The out-of-plane stiffness of the actual floors and roof were calculated, and they were assigned to the corresponding floors and roof in the model. Floors and roof diaphragms connected the top plates of the corresponding storeys together.

3.3.5 Shear wall connectivity at adjacent storeys

In the high-resolution FEM, the bottom plates of upper storey shear walls and top plates of lower storey shear walls were connected through the assumed rigid links (Figure 2-13) at the location of the studs, while the sheathing panels were not connected. The rigid-link-assumption is reasonable because many bolts go through floors to connect the shear walls in the actual building, thus making the floor very stiff with limited deformation. This assumption also aligns with the rigid diaphragm assumption for the floors and roof.

3.4 Validation of the high-resolution FEM through field measurement

NBCC (2015) provides an equation (Equation 3-1) to estimate the natural period of shear wall systems by considering only the building height as a variable. This equation is used for all types of shear wall structures including reinforced concrete, steel and wooden structural systems. Hafeez et al (2018) questioned the suitability of this equation for LFWS because the development of this equation was based on reinforced concrete shear wall building. So, this equation might not be adequate to be used to validate the accuracy of natural period predicted by the 3D high-resolution model.

$$T = 0.05(h_n)^{\frac{3}{4}} \tag{3-1}$$

To perform the validation, the wood-on-concrete composite building mentioned in Section 3.2 was instrumented with vibration sensors by Dr. Ayan Sadhu and his students. Uniaxial accelerometers were used in the study for vibration data collection. The sensors

had a sensitivity of 10 V/g and frequency range of 0.1-100 Hz to capture low-frequency motion of the building under ambient conditions. The layout for the instrumentation is provided in Figure 3-4. Since the building was symmetric, four locations were selected for the instrumentation of ten sensors. The arrow pointing to the right represents the sensors designated to measure translation in the *x*-direction and the arrow pointing upwards represents the sensors measuring the translation in *y*-direction. The dot represents the data measurement in *z*-direction (i.e., vertical direction). Sensor instrumentation on site is shown in Figure 3-5.

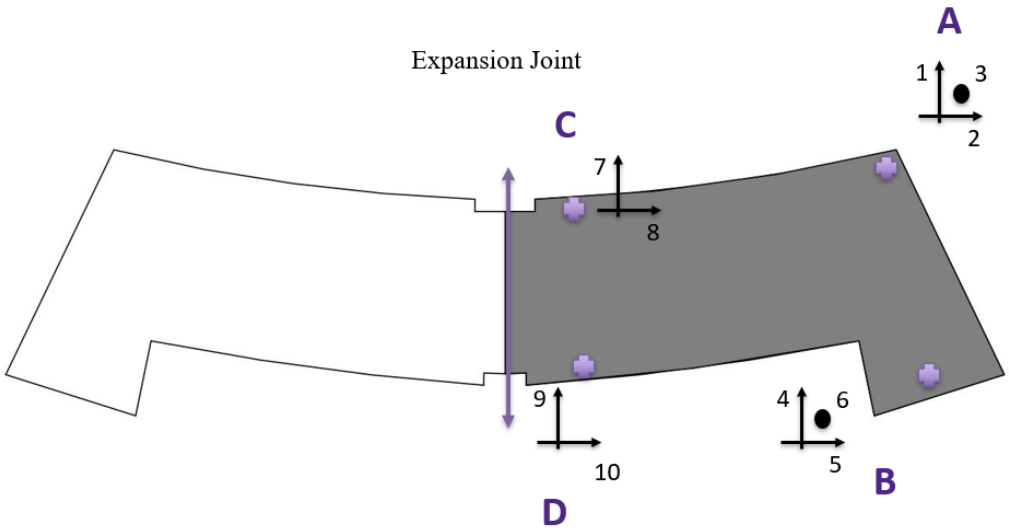

Figure 3-4: Sensor instrumentation plan

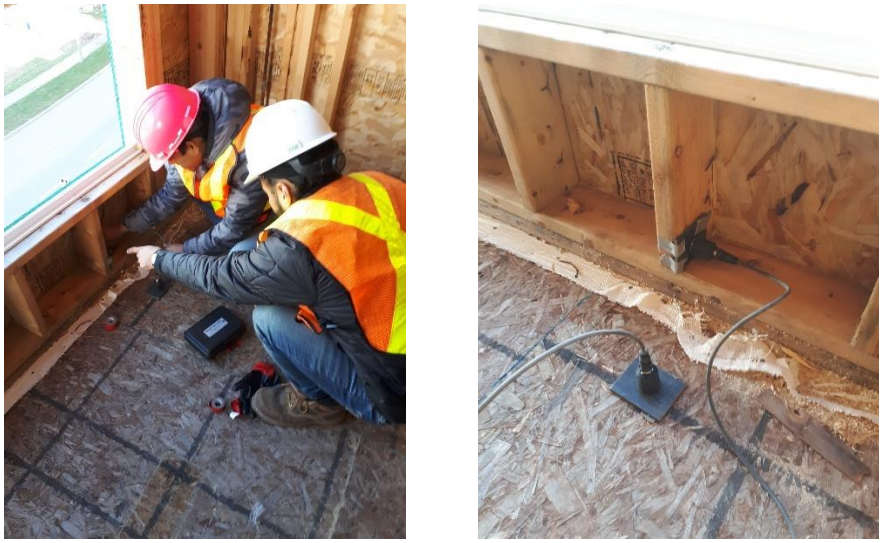

Figure 3-5: On-site sensor instrumentation

Data collection was performed using a data acquisition system by connecting it with the sensor using the BNC cables and with a laptop using a USB cable. The duration of each test was kept to be between 30 seconds to 2 minutes and a sampling frequency of 200 Hz is used.

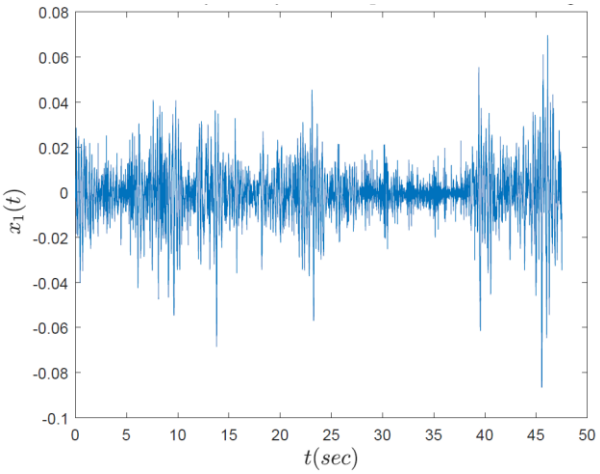

Figure 3-6: Time history of physical response of the top floor of the building

In this study, modal identification was performed using single sensor measurement. The time history of the physical response of the building under a wind gust is shown in Figure 3-6. Dr. Sadhu and his students extracted the mono-component modal responses using system identification method. The mono-component responses and identified structural frequencies are shown in Figure 3-7.

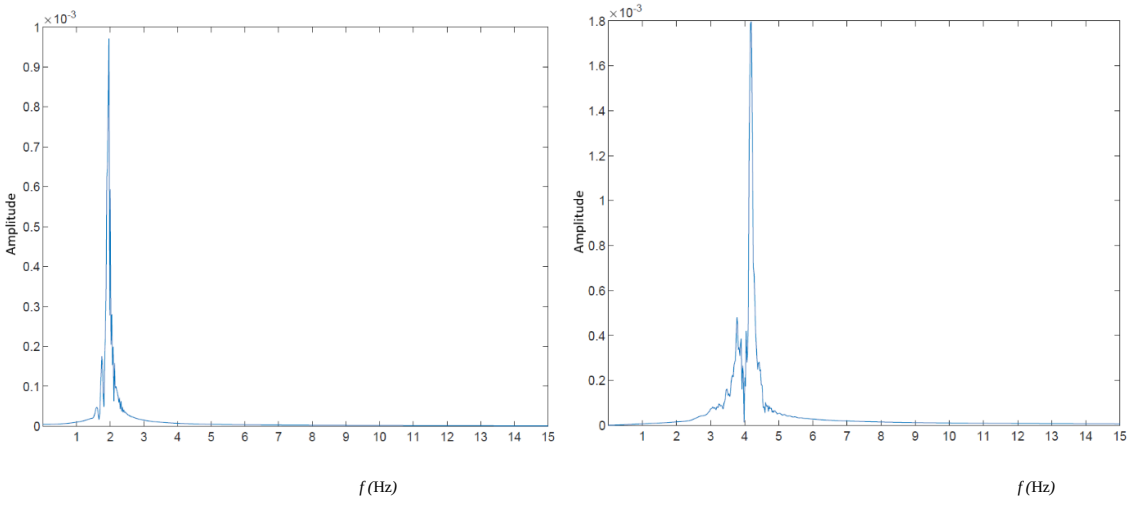

Figure 3-7: Fourier Spectra of modal responses obtained from the field measurement for the first two modes

For the comparison purposes, Table 3-5 shows the first two frequencies from the high-resolution FEM compared with the system identification results. The comparison shows good agreement between the high-resolution FEM and system identification with 10% difference in the first mode and 9.8% difference in the second mode, which validates the accuracy of the 3D four-storey high-resolution model.

Table 3-5: Frequencies comparison

Mode #	FEM	System ID	Difference
1	2.2 Hz	2.0 Hz	10%
2	4.5 Hz	4.1 Hz	9.8%

3.5 Simplified three-dimensional four-storey model

Simplified model for each single-storey shear wall was developed with the simplified FEM procedure mentioned in Chapter 2. The concept of the simplified FEM procedure indicates that no gravity load can be applied on the simplified 3D model after it has been developed, as such gravity load acting on each shear wall was first calculated using tributary area method, and this gravity load was included in the high-resolution model analysis of each shear wall, and subsequently expressed by the properties of the links in the corresponding simplified shear wall. Figure 3-8 shows the simplified 3D four-storey model. Figure 3-9 shows the assumed rigid diaphragm which connects all the joints at the height of a floor in the simplified 3D four-storey model.

Displacement-based pushover analyses were conducted for both the 3D four-storey high-resolution and the simplified models with displacements applied at geometric center of diaphragms. No slabs and roof were modelled in the high-resolution model for this comparison purpose. Gravity loads acting on each shear wall were calculated using tributary area method, and they were added to the shear wall manually in the high-resolution model. The comparison in Figure 3-10 shows very good agreement between both models in terms of pushover analysis. The analyses were conducted using a computer with a processor of Intel Core i7-4790 @ 3.60 GHz, RAM of 16.00 GB, and a solid-state drive speed of 453 MB/s. The analysis required a computational time of 23.5 hours for the high-resolution model, while it required only 41 seconds for the simplified model.

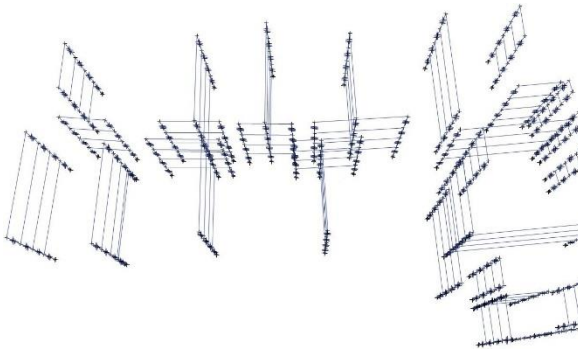

Figure 3-8: Simplified four-storey model

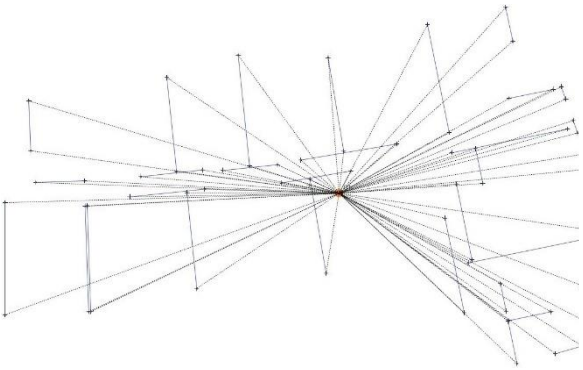

Figure 3-9: Simplified model rigid diaphragm

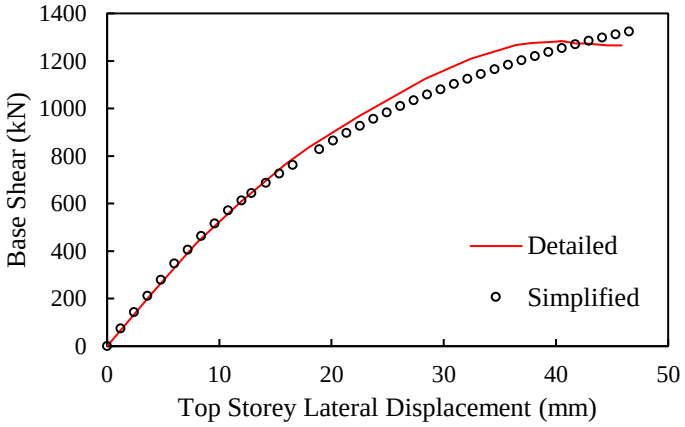

Figure 3-10: Comparison of pushover analyses results for both the high-resolution and simplified model

3.6 Structural performance of the high-resolution model under design loads

Analyzing the 3D multi-storey buildings in ETABS (CSI, 2016) allows for comprehensive understanding of the structural responses with the consideration of system effect, which cannot be captured in experiment or numerical analysis for individual subassembly (i.e., single wall, floor, and one nail). The accuracy of current hand-calculation-based LFWS building design method which conducts the design at single wall level cannot be assessed without the numerical modelling of multi-storey LFWS

buildings at 3D level. A case study was conducted for the building described in Section 3.2 to study the structural performance (i.e., nonlinearity of the nails and the demand-to-capacity ratio of the sheathing panels and frame members) of an actual LFWS building designed based on hand calculation. As a common practice in the high-resolution FEM of LFWS, and also for reducing the complexity of the model, the high-resolution 3D multi-storey LFWS building model in this case study did not include the exterior load bearing walls which are sheathed by GWB.

Each load combination listed in NBCC (2015) was conducted by combining the design loads at one nonlinear load case (Figure 3-11). The longest shear wall W9 (Figure 3-2) with a length of 13.7 m was selected for this study. The most critical deformation (obtained from the envelope load combination of all of the nonlinear load cases which inherently includes the combination of different loads) for the SF and FF nails in the considered DOFs were obtained and shown in Figure 3-12. Obviously, at all of the considered DOFs of both the SF and FF nails, the nails performed in their linear range, so the ductility of these nails were not utilized.

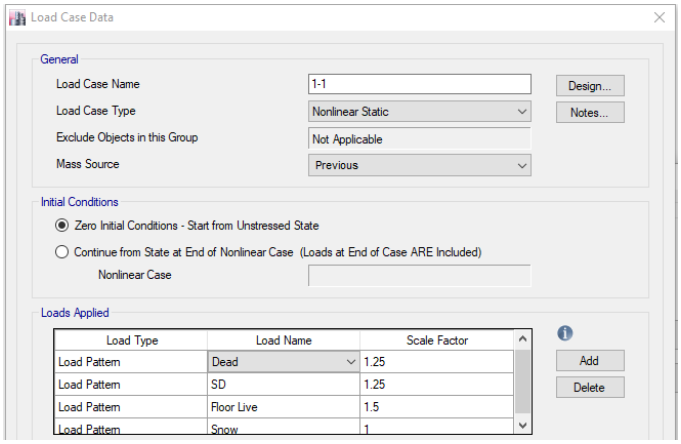

Figure 3-11: Consideration of load combination

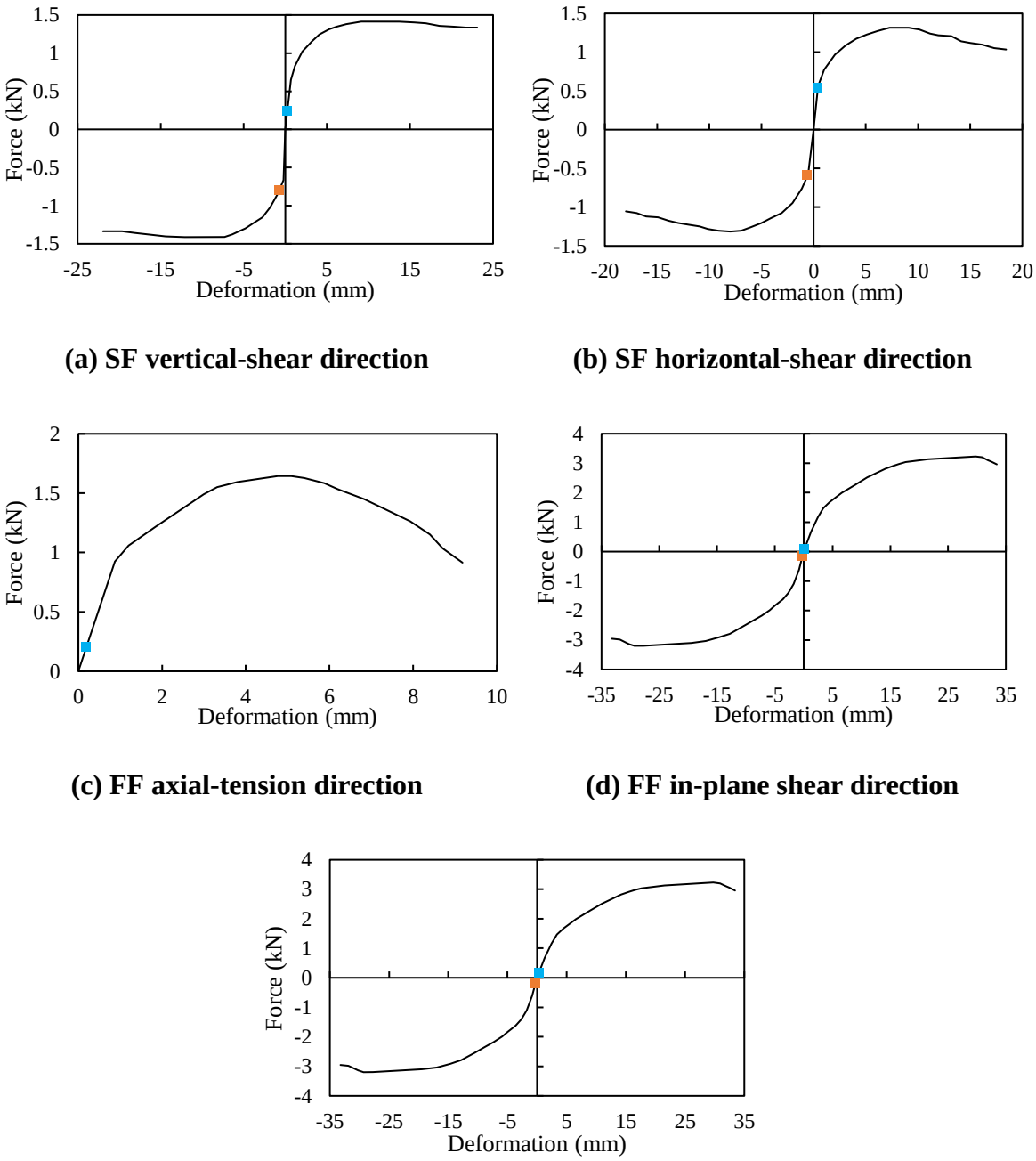

(a) SF vertical-shear direction

(b) SF horizontal-shear direction

(c) FF axial-tension direction

(d) FF in-plane shear direction

(e) FF out-of-plane shear direction

Figure 3-12: Nail deformation under design loads: vertical-shear direction (a) and horizontal-shear direction (b) of SF; axial-tension direction (c), in-plane shear direction (d), and out-of-plane shear direction (e) of FF

Note: black curves are backbone relationships of the nails obtained from Winkel (2006)

The demand-to-capacity ratios of the sheathing panels of the selected shear wall W9 under the most critical load combination were also assessed. Table 3-6 shows the comparisons of the axial-tension and axial-compression force per unit length in both horizontal and vertical directions of the sheathing panels, the in-plane shear force per unit length, and the moment per unit length with respect to the direction parallel to the wall length and the vertical direction obtained from ETABS (CSI, 2016) with Canadian wood design code CSA-O86 (2014). All the demand-to-capacity ratios did not exceed 1. The axial-compression demand-to-capacity ratio in the vertical direction has the largest ratio of 0.7. The out-of-plane bending moment in the direction parallel to the wall length and in the vertical direction has a demand-to-capacity ratio of 0.66 and 0.55, respectively. The demand-to-capacity ratio for axial-compression and the out-of-plane bending moment in reality can be smaller because the external load bearing walls that are sheathed with GWB can carry a portion of the loads, and these walls were not included in the model of this case study for the reason mentioned before. But these ratios can still indicate that the out-of-plane bending effect of the wall cannot be neglected. This out-of-plane bending effect may be caused by the 11.5° inclination of the wall relative to the horizontal *x* axis. The applied *x*-direction lateral load was divided into two components, with one parallel to the wall length and the other one perpendicular to the wall length in the *x*-*y* plane. This obvious out-of-plane bending effect further verifies the necessity of studying the LFWS building at a 3D level with the system effect automatically considered.

Table 3-6: Maximum demand-to-capacity ratios of the sheathing panels of W9

	FEM	Code	Ratio
Axial tension (horizontal) (N / mm)	5.4	30	0.18
Axial tension (vertical) (N / mm)	19.5	60	0.33
Axial compression (horizontal) (N / mm)	14	54	0.26
Axial compression (vertical) (N / mm)	50	71	0.70
In-Plane Shear (N / mm)	9.8	46	0.21
Bending (horizontal) (N · mm / mm)	45	68	0.66
Bending (vertical) (N · mm / mm)	132	240	0.55

Note: The code values were obtained from Table 9.3C of CSA-O86 (2014)

Table 3-7 shows the axial-compression, axial-tension, in-plane moment and in-plane shear demand-to-capacity ratios for the frame members. The critical axial-compression demand-to-capacity ratio was 0.7, this value in reality can be smaller for the same reason mentioned before, which is as a common practice the external load bearing walls that are sheathed with GWB are not modelled to reduce the complexity of the model. Small demand-to-capacity ratios were obtained for axial-tension, in-plane moment, and in-plane shear, indicating the conservativeness of the hand calculation-based design. Particularly, demand-to-capacity ratio for in-plane moment was only 0.02, which indicates that the bending effect of the frame members in LFWS buildings is very small.

Table 3-7: Maximum demand-to-capacity ratios of the frame members of W9

	Axial-compression (kN)	Axial-tension (kN)	In-plane moment (kN · m)	In-plane shear (kN)
FEM	72.1	4.5	0.0806	0.7
Code	102.7	27.6	4.83	5.17
Ratio	0.70	0.16	0.02	0.14

Note: The code strength for axial compression, axial-tension, in-plane moment, and in-plane shear were calculated from Clause 6.5.6.2.3, 6.5.9, 6.5.4.1, and 6.5.5.2, respectively, of CSA-O86 (2014)

3.7 Summary and conclusions

An actual 3D four-storey LFWS building located in Ontario, Canada is first modelled using a high-resolution nonlinear FEM procedure, which simulates all of the shear wall structural components including frame members, sheathing panels, and nails. The developed high-resolution model is validated through frequencies comparison with the field measurement results, which are obtained from system identification method. The simplified FEM procedure for single- and multi-storey shear walls proposed in Section 2 based on the theory of equal work is extended to the modelling of multi-storey LFWS buildings. This 3D simplified model is validated through the pushover analyses on both the high-resolution model and the simplified model of the 3D four-storey building. Subsequently, the validated high-resolution model is further investigated as a case study to assess the structural response under design loads. The nonlinearity of the nails and the

demand-to-capacity ratios for the sheathing panels and the frame members were assessed. The main conclusions of the studies are as follows:

1. The developed high-resolution 3D four-storey model can successfully capture the frequencies with less or equal to 10% difference compared to the field measurement results, which are derived from system identification method.
2. The proposed simplified FEM procedure has the capacity of efficiently and accurately predict the lateral load performance of the 3D four-storey LFWS building. Almost identical pushover analysis results were obtained for both the high-resolution and simplified models with respect to initial stiffness, strength, and ductility.
3. The structural performance assessment of this high-resolution 3D model indicates that the building was over designed, the nails all exhibited linear behaviour, and the design of the frame members and sheathing panels were conservative with small demand-to-capacity ratios. It is also indicated that the frame member in-plane bending effect was small with a demand-to-capacity ratio of 0.02.

3.8 References

ATS. (2008). *Strong-Rod Systems for Multi-Storey Overturning Restraint*. In *Simpson Strong-Tie*.

Baber, T. T., & Noori, M. N. (1985). Random vibration of degrading, pinching systems. *Journal of the Engineering Mechanics Division*, *111*(8), 1010–1026. https://doi.org/10.1061/(ASCE)0733-9399(1985)111:8(1010)

Baber, T. T., & Wen, Y.-K. (1981). Random Vibration Hysteretic, Degrading Systems. *Journal of the Engineering Mechanics Division*, *107*(6), 1069–1087.

Casagrande, D., Rossi, S., Sartori, T., & Tomasi, R. (2012). Analytical and numerical analysis of timber framed shear walls. *World Conference on Timber Engineering 2012*.

Collins, M., Kasal, B., Paevere, P., & Foliente, G. C. (2005a). Three-Dimensional Model of Light Frame Wood Buildings. I: Model Description. *Journal of Structural Engineering*, *131*(4), 676–683. https://doi.org/10.1061/(ASCE)0733-9445(2005)131

Collins, M., Kasal, B., Paevere, P., & Foliente, G. C. (2005b). Three-dimensional model of light frame wood buildings. II: Experimental investigation and validation of analytical model. *Journal of Structural Engineering*, *131*(4), 684–692.

https://doi.org/10.1061/(ASCE)0733-9445(2005)131:4(684)

CSA-O86. (2014). Engineering Design in Wood. In *Canadian Standards Association*. Retrieved from http://shop.csa.ca/en/canada/structures/o86-09-consolidation/invt/27013742009

CSI. (2016). Analysis Reference Manual for SAP2000, ETABS, SAFE and CSiBridge. In *Computers and Structures, Inc.* Retrieved from http://docs.csiamerica.com/manuals/etabs/Analysis Reference.pdf

Filiatrault, A., Isoda, H., & Folz, B. (2003). Hysteretic damping of wood framed buildings. *Engineering Structures*, *25*(4), 461–471. https://doi.org/10.1016/S0141-0296(02)00187-6

Fischer, D., Filiatrault, A., Folz, B., Uang, C.-M., & Seible, F. (2001). Shake Table Tests of a Two-Story Woodframe House. In *CUREE No. W-06*. Richmond, California, USA.

Folz, B., & Filiatrault, A. (2001). Cyclic analysis of wood shear walls. *Journal of Structural Engineering*, *127*(4), 433–441. https://doi.org/10.1061/(ASCE)0733-9445(2001)127:4(433)

Foschi, R. O. (2000). Modeling the hysteretic response of mechanical connections for wood structures. *6th World Conference on Timber Engineering*, 1–11. Whistler, Canada.

Hafeez, G., Doudak, G., & McClure, G. (2018). Establishing the fundamental period of light-frame wood buildings on the basis of ambient vibration tests. *Canadian Journal of Civil Engineering*, *45*(9), 752–765. https://doi.org/10.1139/cjce-2017-0348

Hafeez, G., Doudak, G., & McClure, G. (2019). Dynamic characteristics of light-frame wood buildings. *Canadian Journal of Civil Engineering*, *46*(1), 1–12. https://doi.org/10.1139/cjce-2017-0266

Li, M., Lam, F., Foschi, R. O., Nakajima, S., & Nakagawa, T. (2012). Seismic performance of post and beam timber buildings I: Model development and verification. *Journal of Wood Science*, *58*(1), 20–30. https://doi.org/10.1007/s10086-011-1219-5

Martin, K. G., Gupta, R., Prevatt, D. O., Datin, P. L., & Van De Lindt, J. W. (2011). Modeling system effects and structural load paths in a wood-framed structure. *Journal of Architectural Engineering*, *17*(4), 134–143. https://doi.org/10.1061/(ASCE)AE.1943-5568.0000045

Mi, H. (2004). *Behavior of unblocked wood shear walls* (University of New Brunswick, Fredericton, Canada). Retrieved from http://scholar.google.com/scholar?hl=en&btnG=Search&q=intitle:Behavior+of+unb

locked+wood+shearwalls#1

NBCC. (2015). *National Building Code of Canada*. Ottawa, Canada: National Research Council of Canada.

Niazi, M., El Damatty, A., & Hamada, A. (2018). Sensitivity study of the light-framed wood shear walls subjected to lateral loads. *6th International Structural Specialty Conference 2018, Held as Part of the Canadian Society for Civil Engineering Annual Conference 2018*, 1–9. Fredericton, Canada.

Pei, S., & van de Lindt, J. W. (2009). Coupled shear-bending formulation for seismic analysis of stacked wood shear wall systems. *Earthquake Engineering and Structural Dynamics*, *38*(14), 1631–1647. https://doi.org/10.1002/eqe

Pei, S., & van de Lindt, J. W. (2011). Seismic numerical modeling of a six-story light-frame wood building: Comparison with experiments. *Journal of Earthquake Engineering*, *15*(6), 924–941. https://doi.org/10.1080/13632469.2010.544840

Satheeskumar, N., Henderson, D. J., Ginger, J. D., Humphreys, M. T., & Wang, C. H. (2016). Load sharing and structural response of roof–wall system in a timber-framed house. *Engineering Structures*, *122*, 310–322. https://doi.org/10.1016/j.engstruct.2016.05.009

Satheeskumar, Navaratnam, Henderson, D. J., Ginger, J. D., & Wang, C. H. (2017). Three-Dimensional Finite-Element Modeling and Validation of a Timber-Framed House to Wind Loading. *Journal of Structural Engineering (United States)*, *143*(9). https://doi.org/10.1061/(ASCE)ST.1943-541X.0001850

Smith, S. (2009). *ABAQUS Standard User's Manual, Version 6.9*. Providence, RI.

Stewart, W. G. (1987). *The seismic design of plywood sheathed shear walls*. University of Canterbury, Christchurch, New Zealand.

Tarabia, A. M., & Itani, R. Y. (1997). Static and dynamic modeling of light-frame wood buildings. *Computers & Structures*, *63*(2), 319–334.

Tomasi, R., Sartori, T., Casagrande, D., & Piazza, M. (2015). Shaking table testing of a full-scale prefabricated three-story timber-frame building. *Journal of Earthquake Engineering*, *19*(3), 505–534. https://doi.org/10.1080/13632469.2014.974291

Winkel, M. H. (2006). Behavior of light-frame walls subject to combined in-plane and out of plane loads (University of New Brunswick, Fredericton, Canada). Retrieved from http://scholar.google.com/scholar?hl=en&btnG=Search&q=intitle:Behavior+of+light-frame+walls+subject+to+combined+in-plane+and+out+of+plane+loads#0

Xu, J., & Dolan, J. D. (2009). Development of a wood-frame shear wall model in ABAQUS. *Journal of Structural Engineering*, *135*(8), 977–984.

https://doi.org/10.1061/(ASCE)ST.1943-541X.0000031

Younquist, J. A. (2000). *Wood based composites and panel products: Wood as an engineering material*. Madison, Wis.

Chapter 4

4 Conclusions and Recommendations for Future Work

4.1 Conclusions

The primary concern of this thesis is the development of a high-resolution and a simplified numerical procedure for the lateral load analysis of multi-storey LFWS buildings. To examine the accuracy and to demonstrate the applications of the numerical procedures, a series of studies are performed as listed below.

a) Outline the adopted single wall high-resolution numerical modelling procedure. The procedure has been previously found capable of simulating single- and multi-storey LFWS shear walls with respect to base shear versus lateral displacement predictions.
b) Describe the proposed simplified numerical modelling procedure for single-storey single wall step by step. The theory underlying this procedure is that the work done by the external load equals the work performed by the internal load. Total lateral displacement of the high-resolution numerical model is separated into flexural displacement and shear displacement, which are then transformed into the simplified numerical model's spring properties. The considerations of varied tie rods and gravity loads in the modelling procedure are presented.
c) Establish and run pushover analysis on the high-resolution and simplified numerical models for six single-storey shear walls with varied aspect ratio, tie rods, and gravity loads. Plot the curves of base shear versus different lateral displacement components, and the simplified model's spring properties for each shear wall. These plots are used to study the effect of aspect ratio, tie rod, and gravity load on the structural performance of LFWS shear walls. Compare the pushover analyses results obtained for both the high-resolution and the simplified numerical models for each of the six shear walls to validate the accuracy of the simplified numerical procedure.

d) Extend the single-storey simplified numerical procedure to multi-storey LFWS shear walls. Four four-storey LFWS shear walls with different aspect ratios and tie rods are modelled using both the high-resolution and the simplified multi-storey numerical procedures. Pushover analyses results for each storey of the shear walls obtained from both the high-resolution and the simplified models are compared for the purpose of validating the multi-storey simplified numerical procedure.
e) Extend the adopted single wall high-resolution numerical modelling procedure to model 3D multi-storey LFWS buildings. Use the developed high-resolution 3D modelling method to model an actual complex four-storey LFWS building recently completed in Ontario, Canada, as a case study. The case-studied building is also instrumented in the site to acquire its frequencies using system identification method. These frequencies are compared to the frequencies predicted by the high-resolution model's modal analysis results to validate the accuracy of the developed 3D model of the four-storey LFWS building.
f) Extend the simplified numerical modelling method to 3D buildings. Develop the simplified numerical model for the case-studied four-storey LFWS building. Run displacement-based pushover analyses on both the high-resolution and the simplified models to verify the accuracy of the simplified numerical approach for 3D multi-storey buildings.
g) Perform analyses on the validated high-resolution model for the case-studied building under the design loads to assess the structural performance (nonlinearity of the nails and the demand-to-capacity ratios of the frame members and the sheathing panels) of the building which was designed by hand-calculation-based method.

As mentioned in the first chapter of this thesis, these steps were performed within two chapters, the second and the third. The conclusions derived from the second chapter, titled Simplified Numerical Approach for the Lateral Load Analysis of Light-Frame Wood Shear Wall Structures, can be summarized in the following points:

1. For the six single-storey shear walls with varied structural details, the proposed simplified numerical procedure has the capability of providing almost identical pushover analysis results as those obtained from the high-resolution models.
2. Compared to the high-resolution numerical method, good agreements with respect to pushover analysis are also obtained for multi-storey shear walls modelled using the simplified numerical method. Good accuracy is obtained for a four-storey shear wall with a small aspect ratio (3.5), both with and without tie rods. For the four-storey shear wall with a high aspect ratio (10.5) without tie rods, the simplified numerical model produces 13.2% less strength and a maximum of 15% greater initial stiffness compared to the high-resolution numerical model. This kind of very critical high-aspect-ratio LFWS shear wall are usually strengthened with tie rods in design to reduce the vulnerability of flexural failure. The simplified numerical model is capable of simulating the pushover analysis of the high-aspect-ratio (10.5) four-storey shear wall strengthened with tie rods with almost identical results compared with the high-resolution numerical model.
3. Shear walls with small aspect ratios are more dominated by shear displacement than shear walls with high aspect ratios. Tie rods and gravity loads acting on a wall can significantly increase the flexural stiffness of the wall, as such, making the wall more vulnerable to shear failure. Adding tie rods and gravity loads on large-aspect-ratio shear walls can largely increase the ability resisting lateral loads because the shear strength can be fully utilized without prior flexural failure. The addition of tie rods and gravity loads to small-aspect-ratio shear walls contributes less to the capacity to resist lateral loads.
4. The capacity of a shear wall to resist lateral loads does not increase linearly with wall length. W_L is twice as long as W_S, however, its peak lateral load resistance is 5.9 times greater than that of W_S.

The third chapter of this thesis presented the implementation of the remaining steps listed at the beginning of this chapter. With the tittle of High-resolution and Simplified Numerical Modelling of a Four-Storey Light-Frame Wood Building, the chapter's outcomes can be summarized as follows:

1. The developed high-resolution 3D four-storey model can successfully capture the frequencies with less or equal to 10% difference compared to the field measurement results, which are derived from system identification method.
2. The proposed simplified numerical method can successfully and efficiently conduct pushover analysis on 3D multi-storey LFWS buildings. Good pushover analysis results were obtained for both the high-resolution and simplified models of the case-studied building with respect to initial stiffness, strength, and ductility.
3. Under design loads, the nails in the studied wall of the high-resolution numerical model all exhibited linear behavior, and the demand-to-capacity ratios of the frame members and the sheathing panels were small. This indicates that the hand-calculation-based design of the case-studied building is conservative. Particularly, the largest demand-to-capacity ratio of the frame members due to in-plane bending moment is 0.02, which indicates the frame members' bending effect of this particular shear wall can be neglected.
4. The method adopted in the simplified numerical procedure to separate flexural and shear displacement from the total displacement is accurate. This separation method offers an effective tool for studying the structural performance under different displacement components using either experimental or numerical method.

4.2 Recommendations for future work

Further research should focus on developing the high-resolution and simplified numerical model for the floor/roof systems, as well as establishing a simplified model database with a variety of shear walls and floor/roof structural details to aid the design process of LFWS buildings. The following directions are suggested:

1. Develop a high-resolution numerical procedure for floor systems with all structural details simulated. Verify its accuracy through full-scale filed monitoring.
2. Develop a simplified numerical procedure for floor systems using similar approach in this thesis and validate this simplified procedure by comparing with the high-resolution numerical model for floors.

3. Combine the high-resolution numerical shear wall model with the high-resolution numerical floor model to establish an entire building model. Similar to the high-resolution model combination, a combined simplified numerical model incorporating simplified shear wall model and simplified floor model should also be obtained. The accuracy and efficiency of this simplified entire building model should be validated through pushover analyses on both high-resolution and simplified entire building models.
4. Establish a simplified model database with a variety of shear walls and floor/roof structural details. This database will allow for the design engineers quickly performing the simplified numerical analysis and design. The database can also be substituted by a preprocessor software capable of automatically performing single wall high-resolution modelling and analysis on ETABS once users enter all required structural details on the developed software. The developed software can be further extended so that it can automatically read and extract the ETABS results, and automatically transform them into simplified models on ETABS.
5. Conduct more analyses using the simplified building models (i.e., seismic time-history analysis and wind-induced vibrations with the help of Computational Fluid Dynamics) to accurately assess the structural performance of LFWS buildings subjected to different loads.

Curriculum Vitae

Name:	Chu Peng
Post-secondary Education and Degrees:	South China University of Technology Guangzhou, Guangdong, China 2013-2017 BEng The University of Western Ontario London, Ontario, Canada 2018-2020 MESc
Honours and Awards:	Mitacs Globalink Graduate Fellowship 2018
Related Work Experience	Teaching Assistant The University of Western Ontario 2018-2019

Publications:

Peng, C., El Damatty, A.A., Musa, A., and Hamada, A. Simplified Numerical Approach for the Lateral Load Analysis of Light-Frame Wood Shear Wall Structures, *Engineering Structures* (submitted in Dec. 2019)

Peng, C. and Guner, S. (2018). Direct Displacement-Based Seismic Assessment of Concrete Frames Using Nonlinear Pushover Analysis. *Computers and Concrete*, *21*(4), 355-365.